International Journal of
Cancer and Clinical Research

Original Article: Open Access

Phase I Clinical Study of Survivin-Derived Peptide Vaccine for Patients with Advanced Gastrointestinal Cancers

Fukino Satomi[1], Hiroaki Shima[1], Toru Mizuguchi[1]*, Toshihiko Torigoe[2]*, Goro Kutomi[1], Yasutoshi Kimura[1], Yoshihiko Hirohashi[2], Yasuaki Tamura[2], Tomohide Tsukahara[2], Takayuki Kanaseki[2], Akari Takahashi[2], Hiroko Asanuma[2], Yoichi M. Ito[3], Hiroshi Hayashi[4], Osamu Sugita[4], Noriyuki Sato[2] and Koichi Hirata[1]

[1]Department of Surgery, Surgical Oncology and Science, Sapporo Medical University School of Medicine, Japan

[2]Department of Pathology, Sapporo Medical University School of Medicine, Japan

[3]Department of Biostatistics, Hokkaido University Graduate School of Medicine, Japan

[4]Division of TR Planning and Management, Center for Translational Research, Hokkaido University, Japan

***Corresponding author:** Toru Mizuguchi, MD, PhD, Department of Surgery, Surgical Oncology and Science, Sapporo Medical University School of Medicine, S-1, W-16, Cho-ku, Sapporo, Hokkaido 060-8556, Japan, Tel: +81-11-611-2111 (ext. 3281), Fax: +81-11-613-1678, e-mail: tmizu@sapmed.ac.jp*

Toshihiko Torigoe, MD, PhD, Department of Pathology, Sapporo Medical University School of Medicine, S-1, W-17, Cho-ku, Sapporo, Hokkaido 060-8556, Japan, Tel: +81-11-611-2111 (ext. 2691), Fax: +81-11-643-2310, E-mail: torigoe@sapmed.ac.jp

Abstract

Survivin is a member of the Inhibitor of Apoptosis Protein (IAP) family. It is expressed in fetal tissues but not in normal adult tissues. Since Survivin is over expressed in various types of tumor tissues as well as tumor cell lines, it is considered to be suitable as a target antigen for cancer vaccine therapy. We identified an HLA-A24-restricted antigenic peptide, SVN-2B (AYACNTSTL), derived from a splicing variant of Survivin-2B. In the present study, we carried out a phase I clinical study assessing the safety and efficacy of vaccination with the peptide in patients having advanced gastrointestinal cancer. Vaccinations with 0.1mg, 1.0mg, or 3.0mg doses of the SVN-2B peptide were given subcutaneously four times at 14-day intervals. In 20 patients who received at least one vaccination, grade 1 and grade 2 treatment-related adverse events were observed, including injection site extravasation (grade 2), injection site reaction (grade 1), skin induration (grade 1) and fever (grade 1). No severe adverse event was observed in any patient. Based on tumor size evaluated by computed tomography, eight of the 15 patients who completed the vaccination schedule were considered to have stable disease as assessed by the RECIST criteria. Analysis of peripheral blood lymphocytes using HLA-A24/peptide tetramers revealed the highest increase of SVN-2B-specific cytotoxic T lymphocyte frequency in the 1.0mg dose group. The present clinical study indicates that SVN-2B peptide vaccination is safe and can be considered a potent immunotherapy for HLA-A24-positive gastrointestinal cancer patients.

Keywords

Survivin, Cancer vaccine, Gastrointestinal cancer, Tetramer, Phase I trial

Abbreviations

IAP: Inhibitor of Apoptosis Protein, CTLs: Cytotoxic T lymphocytes, HLA: Human Leukocyte Antigen, CT: Computed Tomography, PBLs: Peripheral Blood Lymphocytes, AEs: Adverse Events, HIV: Human Immunodeficiency Virus, PD: Progressive Disease, SD: Stable Disease, IFN: Interferon

Introduction

Cytotoxic T lymphocytes (CTLs) can recognize MHC class I-bound peptides derived from tumor antigens in cancer cells. Following the first report of the identification of a human tumor antigen, melanoma antigen-1 (MAGE-1), in 1991 [1] a large number of antigenic peptides from various human cancers have been identified [2-7]. They have been employed in immunotherapy for cancer and clinical trials of peptide-based vaccine therapies have taken place [8-11].

We have identified a human leukocyte antigen (HLA)-A24-restricted antigenic peptide, SVN-2B (AYACNTSTL), which was derived from the exon 2B-encoded region of Survivin-2B, a splicing variant of Survivin [12]. Survivin is a member of the inhibitor of apoptosis protein (IAP) family with a single baculovirus IAP repeat domain [13]. It is expressed during fetal development but undetectable in terminally differentiated normal adult tissues. In contrast to normal tissues, Survivin and Survivin-2B are expressed in transformed cell lines and in most common cancers, including gastrointestinal cancer and pancreatic cancer [13,14]. We reported previously that SVN-2B peptide-specific CTLs were increased by

Citation: Satomi F, Shima H, Mizuguchi T, Torigoe T, Kutomi G, et al., (2015) Phase I Clinical Study of Survivin-Derived Peptide Vaccine for Patients with Advanced Gastrointestinal Cancers. Int J Cancer Clin Res 2:012

Received: January 22, 2015: **Accepted:** February 02, 2015: **Published:** February 04, 2015

ClinMed
International Library

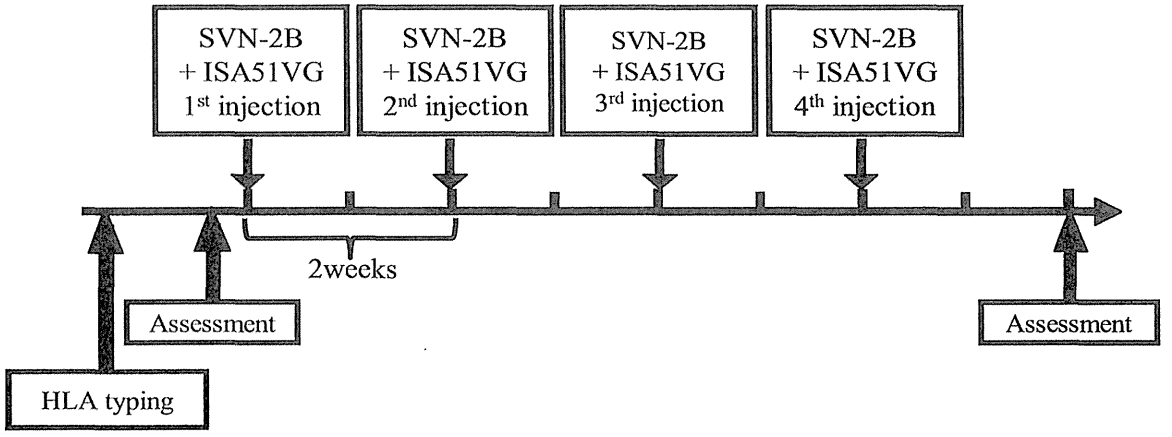

Figure 1: Protocols of the clinical study

The SVN-2B peptide at a dose of 0.1mg/1mL, 1mg/1mL, or 3mg/1mL was emulsified with Montanide ISA51VG at a volume of 0.8mL immediately before vaccination. The patients were then vaccinated subcutaneously (s.c.) four times at 14-day intervals. Tumor size and the immunological response were evaluated before treatment and at two weeks after the 4th vaccination.

stimulating peripheral blood lymphocytes (PBLs) of cancer patients with the peptide *in vitro* [15]. The induced CTLs showed specific cytotoxicity against HLA-A24-positive cancer cells [15-17]. We have carried out clinical trials of SVN-2B vaccination. The SVN-2B peptide was given subcutaneously to patients six times or more at biweekly intervals for colon, breast, oral cavity, and urinary bladder cancer patients [18-24]. There were no severe adverse effects and, clinically, certain patients showed reductions in tumor markers and tumor size as assessed by Computed Tomography (CT). In the present clinical study, we reevaluated the safety and efficacy of SVN-2B vaccination in accordance with good clinical practice guidelines and evaluated the optimal dose of the peptide.

Methods

Patient selection

The study protocol was approved by the Institutional Review Board of Sapporo Medical University. All patients gave informed consent before being enrolled. This study was conducted in accordance with the International Conference on Harmonisation E6 requirements for Good Clinical Practice and with the ethical principles outlined in the Declaration of Helsinki.

Patients enrolled in this study were required to conform to the following criteria: (1) to have histologically confirmed gastrointestinal, bile duct, or pancreatic cancer, (2) to be HLA-A*2402 positive, (3) to have Survivin-positive cancer tissue confirmed by immunohistochemical staining, (4) to be between 20 and 85 years old, (5) to have lesions measureable by CT at the time of registration, (6) to have a history of standard chemotherapy, (7) to have grade 0 or 1 in Eastern Cooperative Oncology Group (ECOG) performance status, and (8) to have no serious organ failure within 30 days at the time of registration.

Exclusion criteria included: (1) prior cancer therapy such as chemotherapy, radiation therapy or other immunotherapy within the previous 4 weeks, (2) presence of other cancers that might influence the prognosis, (3) administration of immunosuppressive drugs such as systemic steroid therapy, (4) severe cardiac insufficiency, acute infection, or hematopoietic failure, (5) uncontrollable diabetes or hypertension, (6) pregnancy or ongoing breast-feeding, and (7) unsuitability for the trial based on clinical judgment. In addition, patients with a high frequency of the peptide-specific CTLs at the time of registration were excluded since such patients were poor responders to the vaccine in our previous studies [23,24]. The number of the HLA-A24/SVN-2B peptide tetramer-positive CTLs per 10,000 CD8-positive T cells (CTLpre) was analyzed at the time of registration and patients who had a value of log10 (1+CTLpre) higher than 1.6 were excluded.

Peptide preparation

The peptide SVN-2B with the sequence **AYACNTSTL** was prepared under good manufacturing practice conditions by PolyPeptide Laboratories San Diego (San Diego, CA, USA). The identity of the peptide was confirmed by mass spectral analysis, and the purity was shown to be more than 98% as assessed by high pressure liquid chromatography analysis. The peptide was supplied as a freeze-dried, sterile white powder. It was dissolved in 1.0 ml of physiological saline (Ohtsuka Pharmaceutical Co., Ltd., Tokyo, Japan) and stored at -80°C until just before use.

Patient treatment

This study was carried out as an open-label, randomized parallel group study at the Department of Surgery, Surgical Oncology and Science of Sapporo Medical University Hospital to evaluate the safety and efficacy of the SVN-2B peptide vaccine for patients who had advanced or recurrent gastrointestinal or pancreatic cancer (UMIN000008611). The patients were randomly assigned into the following three dosage groups: group 1 patients received 0.1mg, group 2 received 1.0mg and group 3 received 3mg. Each group included five patients. SVN-2B at a dose of 0.1mg/1mL, 1mg/1mL, or 3mg/1mL was emulsified with Montanide ISA51VG (Seppic, Paris, France) at a volume of 0.8mL immediately before vaccination. The patients were then vaccinated subcutaneously (s.c.) four times at 14-day intervals (Figure 1).

Toxicity evaluation

Patients were examined closely for signs of toxicity during and after vaccination. Adverse events (AEs) were recorded using CTCAE (version 4.03) criteria and graded for severity.

Clinical response evaluation

Physical and hematological examinations were conducted before and after each vaccination. Changes in tumor marker levels (CEA and CA19-9) were evaluated by comparison of the serum levels before the first vaccination and those after the fourth vaccination. Tumor size was evaluated by CT scans before treatment and at two weeks after the fourth vaccination (Figure 1). The antitumor response was evaluated according to the Response Evaluation Criteria in Solid Tumors (RECIST: version 1.1) guideline [25]. Briefly, a complete response (CR) was defined as complete disappearance of all measurable and evaluable disease. A partial response (PR) was defined as a >=30%

Table1: Profiles of patients in the full analysis set for safety assessment (N=20)

Clinical variables		0.3 mg (n=7)	1.0 mg (n=7)	3.0 mg (n=6)	Total (n=20)
Gender	Men: Women	2:5	5:2	3:3	10:10
Age	Median (min-max)	69.5 (53-80)	63.0 (51-84)	64.4 (41-66)	65.1(41-84)
Type of cancer	Pancreatic cancer	5	2	5	12
	Colon cancer	2	3	1	6
	Gastric cancer	0	1	0	1
	Bile duct cancer	0	1	0	1
Metastasis	(positive: negative)	7:0	5:2	5:1	17:3
Prior surgery	(positive: negative)	4:3	5:2	3:3	12:8
Prior radiation therapy	(positive: negative)	2:5	2:5	3:3	7:13
Prior chemotherapy	(positive: negative)	6:1	6:1	6:0	18:2
ECOG PS	(0:1)	1:6	1:6	2:4	4:16
Treatment-related AEs					
Fever	Grade 1	1			1
Injection site extravasation	Grade 2			1	1
Injection site reaction	Grade 1	1		1	2
Skin induration	Grade 1	1	1		2

decrease from baseline in the size of all measurable lesions (sum of maximal diameters). Progressive disease (PD) was defined as an increase in the sum of maximal diameters by at least 20% or the appearance of new lesions. Stable disease (SD) was defined as the absence of criteria matching those for CR, PR or PD. Patients who received fewer than four vaccinations were excluded from clinical response evaluations in this study.

In vitro stimulation of PBLs

PBLs were isolated by Ficoll-Conray density gradient centrifugation using Lymphoprep (AXIS-SHIELD, Oslo, Norway). They were then frozen and stored at -80°C. The frozen PBLs were thawed and incubated in the presence of 40μg/mL SVN-2B in AIM-V medium (Life Technologies, Carlsbad, CA, USA) containing 10% human serum at room temperature. Next, interleukin-2 was added at a final concentration of 50 U/mL 1 hour, 2 days and 4 days after addition of the peptide. On day 7 of culture, the PBLs were analyzed by tetramer staining assay and ELISPOT assay.

Tetramer staining

FITC-labeled HLA-A*2402/human immunodeficiency virus (HIV)-derived peptide (RYLRDQQLL) and PE-labeled HLA-A*2402/SVN-2B peptide tetramers were purchased from MBL, Inc. (Nagoya, Japan). For flow cytometric analysis, PBLs, which were stimulated *in vitro* as above, were stained with the FITC-labeled tetramer and PE-labeled tetramer at 37°C for 20 min, followed by staining with a PC5-labeled anti-CD8 monoclonal antibody (Beckton Dickinson Biosciences, San Jose, CA, USA) at 4°C for 30 min. The cells were washed twice with PBS before fixation in 1% formaldehyde. Flow cytometric analysis was performed using FACSCalibur and CellQuest software (Beckton Dickinson Biosciences). The frequency of CTL precursors was calculated as the number of HLA-A24/SVN-2B tetramer-positive cells per 10,000 CD8-positive cells.

ELISPOT assay

ELISPOT plates were coated sterilely overnight with an IFN-γ capture antibody (Beckton Dickinson Biosciences) at 4°C. The plates were then washed once and blocked with AIM-V medium containing 10% human serum for 2 h at room temperature. CD8-positive T cells separated from patients' PBLs ($5x10^3$ cells/well), which were stimulated *in vitro* as above, were then added to each well along with HLA-A24-transfected CIR cells (CIR-A24) ($5x10^4$ cells/well) preincubated with SVN-2B (10ng/mL, 100ng/mL, 10μg/mL) or the HIV peptide (RYLRDQQLL) as a negative control. After incubation in a 5% CO_2 humidified chamber at 37°C for 24 h, the wells were washed vigorously five times with PBS and incubated with a biotinylated anti-human IFN-γ detection antibody (Beckton Dickinson Biosciences) and horseradish peroxidase-conjugated avidin. Spots were visualized and analyzed using KS ELISPOT (Carl Zeiss, Jena, Germany).

Immunohistochemistry

Immunohistochemical study of the HLA class I expression in the patients' primary cancer tissues was done with anti-HLA class I heavy chain monoclonal antibody EMR8-5 according to the standard methods described previously [26].

Statistical analysis

All statistical analyses were done using SAS Version 9.3 and JMP Version 11.0 (SAS Institute, Inc.). For the tetramer assay, statistical analysis was performed using a one-sided t-test. Statistical analysis of ELISPOT assay was performed using the student t-test.

Results

Patient profiles

From August 2012 to May 2013, 38 patients were assessed for eligibility and 21 patients were initially enrolled in this trial (Figure 2). However, one patient was withdrawn before the first vaccination due to deterioration of the systemic condition. Twenty patients who received at least one vaccination were evaluated for safety as a full analysis set (FAS). Five patients discontinued halfway through the protocol due to progression of the disease. None of the interruptions was due to treatment-related AEs. Fifteen patients received the complete regimen including four vaccinations and were evaluated for efficacy of the vaccine (Figure 2). The patient profiles are shown in Table 1. The primary malignant tumors of the 20 patients were 12 pancreatic cancers, 6 colon cancers (including 2 appendix cancers), 1 gastric cancer and 1 bile duct cancer.

Safety

Peptide vaccination was well tolerated in all patients. The treatment-related AEs are listed in Table 1. They included injection site extravasation (grade 2), injection site reaction (grade 1), skin induration (grade 1) and fever (grade 1). No serious toxicity-associated adverse event was observed during or after the vaccination.

Clinical responses

Table 2 summarizes the clinical outcomes of the 15 patients who received the complete regimen. CT evaluation of tumor size showed that 8 patients had SD and 7 patients PD, although none had PR or

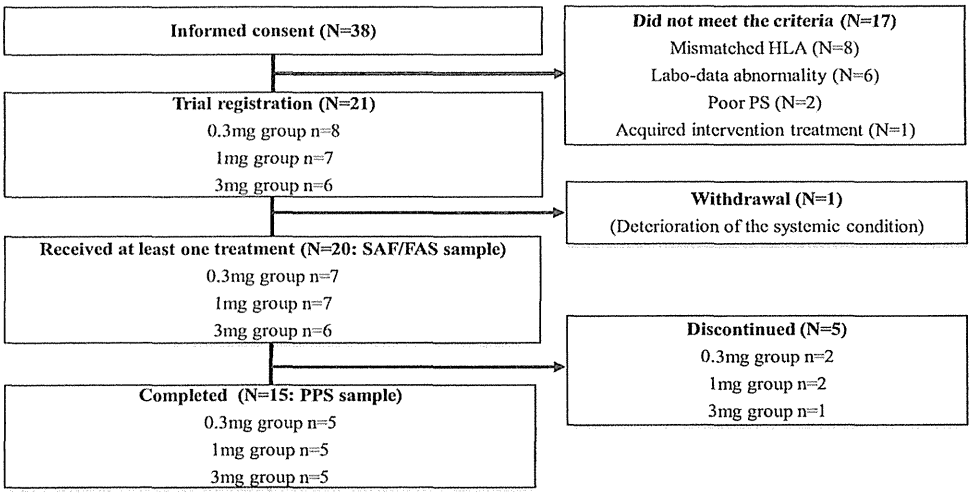

Figure 2: Enrollment of patients

Thirty-eight patients were assessed for eligibility and 21 were initially enrolled in this trial. One patient was withdrawn before the first vaccination due to deterioration of the systemic condition. Twenty patients who received at least one vaccination were evaluated for safety as the full analysis set. Five patients discontinued halfway through the protocol due to progression of the disease. Fifteen patients received the complete regimen and were evaluated for efficacy of the vaccine as the per protocol set. SAF: Safety Analysis Set, FAS: Full Analysis Set, PPS: Per Protocol Set, HLA: Human Leukocyte Antigen, PS: Performance Status.

Table 2: Profiles and clinical outcomes of patients who completed the regimen

Clinical Background						Immunological Response		Antitumor Response		
Dose	Age	Gender	Origin	Status	HLA class I	Tetramer increase	ELISPOT increase	RECIST	CEA	CA19-9
0.3 mg	63	Woman	Pancreas	Inoperable	+	35	-17	**SD**	**Decreased**	**Decreased**
0.3 mg	69	Woman	Pancreas	Inoperable	+	5	-31	**SD**	WNL	Increased
0.3 mg	53	Woman	Pancreas	Post-op	-	7	6	PD	Increased	Increased
0.3 mg	68	Man	Pancreas	Post-op	+	8	17	PD	Increased	Increased
0.3 mg	78	Man	Colon	Post-op	+	-4	2	PD	Increased	Increased
1.0 mg	61	Man	Pancreas	Inoperable	+	21	-1	**SD**	Increased	Increased
1.0 mg	84	Woman	Colon	Post-op	+	28	14	**SD**	Increased	Increased
1.0 mg	69	Man	Stomach	Post-op	+	7	26	**SD**	Increased	Increased
1.0 mg	59	Man	Colon	Post-op	+	29	16	PD	Increased	Increased
1.0 mg	62	Man	Colon	Post-op	+	15	2	PD	Increased	WNL
3.0 mg	41	Woman	Pancreas	Post-op	+	12	158	**SD**	WNL	**Stable**
3.0 mg	66	Man	Pancreas	Inoperable	+	9	19	**SD**	**Decreased**	Increased
3.0 mg	64	Man	Pancreas	Post-op	+	2	-16	**SD**	WNL	**Decreased**
3.0 mg	50	Man	Pancreas	Post-op	+	9	21	PD	WNL	Increased
3.0 mg	64	Woman	Pancreas	Inoperable	+	0	10	PD	Increased	Increased

Post-op: Post-Operative, SD: Stable Disease, PD: Progressive Disease, WNL: Within the Normal Limit

CR. The disease control rate was 53.3%. Among the 8 patients who were defined as having SD, the CEA levels and the CA19-9 levels were decreased or at least stable during vaccination in 2 patients and 3 patients, respectively. The CEA levels stayed within the normal range (0~5.9ng/ml) throughout the study in 4 patients, and the CA19-9 level stayed within the normal range (0~37 U/ml) in one patient. It was noted that all three patients who had undergone immunotherapy before the registration had PD. Moreover, the result for one patient who had HLA class I-negative cancer tissue was also PD.

Tetramer assay and ELISPOT assay

We investigated whether the SVN-2B peptide vaccination could actually induce specific immune responses in the enrolled patients. The peptide-specific CTL frequencies in PBLs before the first vaccination (CTLpre) and after the fourth vaccination (CTLpost) were assessed using the HLA-A24/SVN-2B tetramer, and the tetramer increase (CTLpost-CTLpre) was calculated (Table 2). The HLA-A24/HIV peptide (RYLRDQQLL) tetramer was used as a negative control. SVN-2B-specific CTL frequencies were increased after the vaccination in all patients except two who had undergone immunotherapy before the registration. We compared the tetramer increases between the PD group (non-responders) and SD group (responders). The mean tetramer increase of the SD group was higher than that of the PD group (Figure 3A), although there was no statistical significance

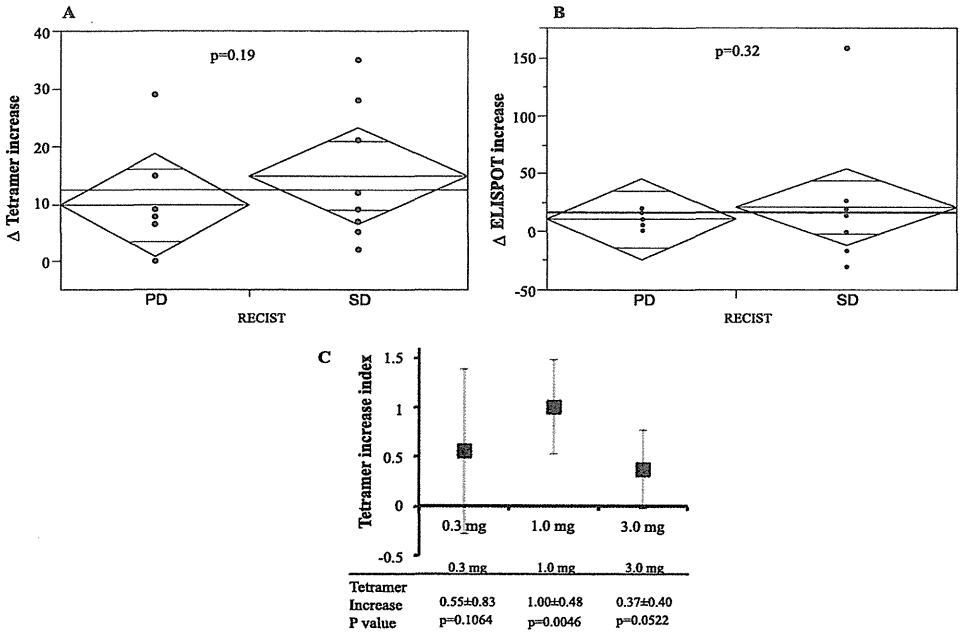

Figure 3: Tetramer assay and ELISPOT assay

(A) The tetramer increase (CTLpost-CTLpre) was calculated from the peptide-specific CTL frequency in PBLs before the first vaccination (CTLpre) and after the fourth vaccination (CTLpost) using the HLA-A24/SVN-2B tetramer. The mean tetramer increases of the PD (non-responders) and SD groups (responders) were compared. (B) The ELISPOT increase was calculated from the numbers of the peptide-specific IFN-γ spots before the first vaccination and after the fourth vaccination. The mean ELISPOT increases of the PD and SD groups were compared. (C) The mean tetramer increase index was calculated according to the following formula: Tetramer increase index=Log10(1+CTLpost)-Log10(1+CTLpre). The mean tetramer indices of the three groups (0.1mg dose, 1.0mg dose, and 3.0mg dose) were compared.

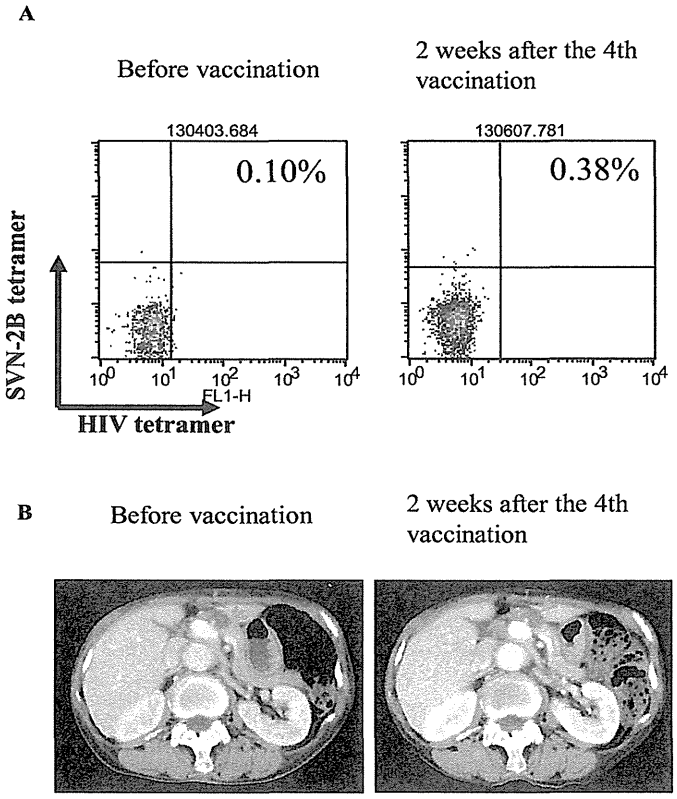

Figure 4: Tetramer assay and CT scan images of the patient with a metastatic pancreatic tumor

An 84-year-old woman with primary colon cancer and metastatic pancreatic tumor. (A) Tetramer assay before vaccination (left panel) and 2 weeks after the 4th vaccination (right panel). (B) CT scan images before vaccination (left panel) and 2 weeks after the 4th vaccination (right panel). The arrowhead indicates the metastatic pancreatic tumor. The tumor grew slightly from 16 mm to 17mm during the 8 weeks of the study.

(p=0.19). To determine the optimal dose of the peptide to induce specific CTLs in patients, the mean tetramer increase indices of the three groups (0.1mg dose, 1.0mg dose, and 3.0mg dose) were compared (Figure 3C). It was found that 1.0mg was the most effective dose for the induction of peptide-specific T cells after the fourth vaccination (p=0.0046).

We also analyzed the peptide-specific IFN-γ responses of CD8-positive T cells by ELISPOT assay. The HIV peptide (RYLRDQQLL) was used as a negative control. The numbers of peptide-specific IFN-γ spots before the first vaccination and after the fourth vaccination were counted, and the ELISPOT increase was calculated (Table 2). There was no significant difference in the mean ELISPOT increase between the SD group and PD group (Figure 3B).

Overall, this study suggests that the immunological response of the vaccine is well represented by tetramer assay rather than ELISPOT assay and that the immunological responses, at least in some patients, appropriately reflect the antitumor responses.

A Case Study

An 84-year-old woman who had primary colon cancer and metastatic liver and pancreatic tumors received the 1.0 mg dose of the SVN-2B vaccine. CT images and tetramer staining data are shown in Figure 4. In this case, the clinical response was defined as SD, and the peptide-specific CTL frequency was increased after the vaccination (Figure 4A). The metastatic pancreatic tumor barely changed from 16 mm to 17 mm during the 8 weeks of the study (Figure 4B). She continued the vaccination after the study. After 6 months, the pancreatic tumor size had increased by 31%, and a new lesion appeared in the caudate lobe of the liver. The time to progression was 267 days. There was no treatment-related AE and she could maintain high quality of daily life for almost one and a half years.

Discussion

The present study demonstrated the safety and clinical efficacy of the survivin-2B peptide vaccine for patients with advanced gastrointestinal cancer. However, the efficacy of vaccination with the SVN-2B peptide plus oil adjuvant Montanide ISA51VG was limited and not sufficient to elicit overt clinical responses. It is obvious that superior clinical and immunological responses are necessary for cancer immunotherapy. It should be considered that vaccination in combination with immunostimulatory adjuvants or cytokines may lead to greater immune and clinical responses. We have reported that type I interferon (IFN) can enhance the antitumor and immunological responses of the peptide vaccine [19,20]. On the basis of the results in this phase I study, we have started a phase II study of the SVN-2B peptide vaccine in combination with IFN-γ.

Immunomonitoring revealed that the tetramer increases were well correlated with antitumor responses as compared with ELISPOT analysis. Therefore, we used the tetramer increase as an index of vaccine-specific immune responses and determined the optimal peptide dose. A significantly higher frequency of tetramer-positive CTLs was induced in the 1mg dose group. However, the optimal dose may vary depending on conditions such as the vaccination interval and combination with distinct adjuvants and/or cytokines, and may have to be reevaluated in combination with IFN. It is enigmatic why the 3mg dose vaccination caused less induction of the peptide-specific CTLs. It was reported previously that persistent vaccine depots could induce sequestration, dysfunction and depletion of antigen-specific CTLs [27]. That may explain, at least in part, the mechanism of the bell-shaped dose effect of the antigenic peptide.

Three patients with a history of immunotherapy such as a dendritic cell vaccine and certain peptide vaccine failed to respond to the SVN-2B peptide vaccine clinically and immunologically. It is possible that their cancers may have had immunoescape phenotypes, thereby maintaining resistance to the vaccine as well as the prior immunotherapy. Alternatively, prior immunotherapy might have affected the immune system, thereby inducing tolerance against the vaccination. In any case, a history of immunotherapy was considered to be a predictive factor for a worse response, and was therefore added to the exclusion criteria in the ongoing phase II clinical study.

In conclusion, we demonstrated the safety and clinical efficacy of the SVN-2B peptide vaccine for patients with advanced gastrointestinal cancer, although clinical interpretation of the results was limited due to this being a phase I study with a small number of patients. At present, a phase II study (UMIN000012146) of the SVN-2B peptide vaccine for advanced pancreatic cancer is ongoing in combination with IFN-γ.

Acknowledgments

This work was supported by Grants-in-Aid for Scientific Research from the Ministry of Education, Culture, Sports, Science and Technology of Japan (grant Nos. 16209013, 17016061 and 15659097) for Practical Application Research from the Japan Science and Technology Agency, and for Cancer Research (15-17 and 19-14) from the Ministry of Health, Labor and Welfare of Japan, Ono Cancer Research Fund and Takeda Science Foundation. This work was supported in part by the National Cancer Center Research and Development Fund (23-A-44) and the Grant for Joint Research Project of the Institute of Medical Science, the University of Tokyo.

References

1. van der Bruggen P, Traversari C, Chomez P, Lurquin C, De Plaen E, et al. (1991) A gene encoding an antigen recognized by cytolytic T lymphocytes on a human melanoma. Science 254: 1643-1647.
2. Nakatsugawa M, Horie K, Yoshikawa T, Shimomura M, Kikuchi Y, et al. (2011) Identification of an HLA-A*0201-restricted cytotoxic T lymphocyte epitope from the lung carcinoma antigen, Lengsin. Int J Oncol 39: 1041-1049.
3. Honma I, Torigoe T, Hirohashi Y, Kitamura H, Sato E, et al. (2009) Aberrant expression and potency as a cancer immunotherapy target of alpha-methylacyl-coenzyme A racemase in prostate cancer. J Transl Med 7: 103.
4. Kawaguchi S, Tsukahara T, Ida K, Kimura S, Murase M, et al. (2012) SYT-SSX breakpoint peptide vaccines in patients with synovial sarcoma: a study from the Japanese Musculoskeletal Oncology Group. Cancer Sci 103: 1625-1630.
5. Sato E, Torigoe T, Hirohashi Y, Kitamura H, Tanaka T, et al. (2008) Identification of an immunogenic CTL epitope of HIFPH3 for immunotherapy of renal cell carcinoma. Clin Cancer Res 14: 6916-6923.
6. Tsukahara T, Kawaguchi S, Torigoe T, Takahashi A, Murase M, et al. (2009) HLA-A*0201-restricted CTL epitope of a novel osteosarcoma antigen, papillomavirus binding factor. J Transl Med 7: 44.
7. Hariu H, Hirohashi Y, Torigoe T, Asanuma H, Hariu M, et al. (2005) Aberrant expression and potency as a cancer immunotherapy target of inhibitor of apoptosis protein family, Livin/ML-IAP in lung cancer. Clin Cancer Res 11: 1000-1009.
8. Rosenberg SA (1999) A new era for cancer immunotherapy based on the genes that encode cancer antigens. Immunity 10: 281-287.
9. Tsuruma T, Hata F, Furuhata T, Ohmura T, Katsuramaki T, et al. (2005) Peptide-based vaccination for colorectal cancer. Expert Opin Biol Ther 5: 799-807.
10. Kawaguchi S, Wada T, Ida K, Sato Y, Nagoya S, et al. (2005) Phase I vaccination trial of SYT-SSX junction peptide in patients with disseminated synovial sarcoma. J Transl Med 3: 1.
11. Asahara S, Takeda K, Yamao K, Maguchi H, Yamaue H (2013) Phase I/II clinical trial using HLA-A24-restricted peptide vaccine derived from KIF20A for patients with advanced pancreatic cancer. J Transl Med 11: 291.
12. Hirohashi Y, Torigoe T, Maeda A, Nabeta Y, Kamiguchi K, et al. (2002) An HLA-A24-restricted cytotoxic T lymphocyte epitope of a tumor-associated protein, survivin. Clin Cancer Res 8: 1731-1739.
13. Ambrosini G, Adida C, Altieri DC (1997) A novel anti-apoptosis gene, survivin, expressed in cancer and lymphoma. Nat Med 3: 917-921.
14. Asanuma H, Torigoe T, Kamiguchi K, Hirohashi Y, Ohmura T, et al. (2005) Survivin expression is regulated by coexpression of human epidermal growth factor receptor 2 and epidermal growth factor receptor via phosphatidylinositol 3-kinase/AKT signaling pathway in breast cancer cells. Cancer Res 65: 11018-11025.
15. Idenoue S, Hirohashi Y, Torigoe T, Sato Y, Tamura Y, et al. (2005) A potent immunogenic general cancer vaccine that targets survivin, an inhibitor of apoptosis proteins. Clin Cancer Res 11: 1474-1482.
16. Kitamura H, Torigoe T, Honma I, Asanuma H, Nakazawa E, et al. (2006) Expression and antigenicity of survivin, an inhibitor of apoptosis family member, in bladder cancer: implications for specific immunotherapy. Urology 67: 955-959.
17. Kobayashi J, Torigoe T, Hirohashi Y, Idenoue S, Miyazaki A, et al. (2009) Comparative study on the immunogenicity between an HLA-A24-restricted cytotoxic T-cell epitope derived from survivin and that from its splice variant survivin-2B in oral cancer patients. J Transl Med 7: 1.
18. Honma I, Kitamura H, Torigoe T, Takahashi A, Tanaka T, et al. (2009) Phase I clinical study of anti-apoptosis protein survivin-derived peptide vaccination for patients with advanced or recurrent urothelial cancer. Cancer Immunol Immunother 58: 1801-1807.

19. Kameshima H, Tsuruma T, Kutomi G, Shima H, Iwayama Y, et al. (2013) Immunotherapeutic benefit of Î±-interferon (IFNÎ±) in survivin2B-derived peptide vaccination for advanced pancreatic cancer patients. Cancer Sci 104: 124-129.

20. Kameshima H, Tsuruma T, Torigoe T, Takahashi A, Hirohashi Y, et al. (2011) Immunogenic enhancement and clinical effect by type-I interferon of anti-apoptotic protein, survivin-derived peptide vaccine, in advanced colorectal cancer patients. Cancer Sci 102: 1181-1187.

21. Miyazaki A, Kobayashi J, Torigoe T, Hirohashi Y, Yamamoto T, et al. (2011) Phase I clinical trial of survivin-derived peptide vaccine therapy for patients with advanced or recurrent oral cancer. Cancer Sci 102: 324-329.

22. Tanaka T, Kitamura H, Inoue R, Nishida S, Takahashi-Takaya A, et al. (2013) Potential survival benefit of anti-apoptosis protein: survivin-derived peptide vaccine with and without interferon alpha therapy for patients with advanced or recurrent urothelial cancer--results from phase I clinical trials. Clin Dev Immunol 2013: 262967.

23. Tsuruma T, Hata F, Torigoe T, Furuhata T, Idenoue S, et al. (2004) Phase I clinical study of anti-apoptosis protein, survivin-derived peptide vaccine therapy for patients with advanced or recurrent colorectal cancer. J Transl Med 2: 19.

24. Tsuruma T, Iwayama Y, Ohmura T, Katsuramaki T, Hata F, et al. (2008) Clinical and immunological evaluation of anti-apoptosis protein, survivin-derived peptide vaccine in phase I clinical study for patients with advanced or recurrent breast cancer. J Transl Med 6: 24.

25. Eisenhauer EA, Therasse P, Bogaerts J, Schwartz LH, Sargent D, et al. (2009) New response evaluation criteria in solid tumours: revised RECIST guideline (version 1.1). Eur J Cancer 45: 228-247.

26. Torigoe T, Asanuma H, Nakazawa E, Tamura Y, Hirohashi Y, et al. (2012) Establishment of a monoclonal anti-pan HLA class I antibody suitable for immunostaining of formalin-fixed tissue: unusually high frequency of down-regulation in breast cancer tissues. Pathol Int 62: 303-308.

27. Hailemichael Y, Dai Z, Jaffarzad N, Ye Y, Medina MA, et al. (2013) Persistent antigen at vaccination sites induces tumor-specific CD8(+) T cell sequestration, dysfunction and deletion. Nat Med 19: 465-472.

Cancer-Associated Oxidoreductase ERO1-α Drives the Production of Tumor-Promoting Myeloid-Derived Suppressor Cells via Oxidative Protein Folding

Tsutomu Tanaka,*,† Toshimitsu Kajiwara,* Toshihiko Torigoe,* Yoshiharu Okamoto,‡ Noriyuki Sato,* and Yasuaki Tamura§

Endoplasmic reticulum disulfide oxidase ERO1-α plays a role in the formation of disulfide bonds in collaboration with protein disulfide isomerase. Disulfide bond formation is required for the proper conformation and function of secreted and cell surface proteins. We found that ERO1-α was overexpressed in a variety of tumor types; therefore, we examined its role in tumor growth. In BALB/c mice, knockdown of ERO1-α within 4T1 mouse mammary gland cancer (KD) cells caused retardation of in vivo tumor growth compared with tumor growth of scrambled control (SCR) cells. In contrast, when ERO1-α–overexpressed 4T1 (OE) cells were compared with mock control cells, OE cells showed augmented tumor growth. However, differences in tumor growth were not observed among four groups of nude mice, suggesting that expression of ERO1-α diminished antitumor immunity. We observed dense peritumoral granulocytic infiltrates in tumors of wild-type 4T1 and SCR cells but not KD cells, and these cells were identified as polymorphonuclear myeloid-derived suppressor cells (MDSCs). In addition, production of G-CSF and CXCL1/2, which have intramolecular disulfide bonds, from KD cells was significantly decreased compared with that from SCR cells. In contrast, OE cells produced a larger amount of these molecules than did mock cells. These changes were regulated at the posttranscriptional level. These results suggest that overexpression of ERO1-α in the tumor inhibits the T cell response by recruiting polymorphonuclear MDSCs via regulation of MDSC-prone cytokines and chemokines. ***The Journal of Immunology*****, 2015, 194: 2004–2010.**

The tumor microenvironment was shown to be an immunosuppressive microenvironment. Myeloid-derived suppressor cells (MDSCs) are a major component of the immune-suppressive network in cancer and many other pathological conditions. Experimental models using mice showed that MDSCs can facilitate tumor progression by promoting the suppression of antitumor immunity (1–4), promoting inflammation (4, 5), stimulating angiogenesis (6), and enhancing tumor cell migration and metastasis (7). Clinical studies further demonstrated that the presence of MDSCs correlates with adverse outcomes and shorter survival in various types of cancer, including breast cancer (8). MDSCs are a heterogeneous group of myeloid cells that are characterized by potent immunosuppressive activity. In mice, they are characterized as $CD11b^+$ $Gr\text{-}1^+$ cells. In recent years, two major groups of cells that make up MDSCs have been identified: cells with a morphology and phenotype ($CD11b^+$ $Ly6C^{low}$ $Ly6G^+$) typical of polymorphonuclear (PMN)-MDSCs and cells with a morphology and phenotype ($CD11b^+$ $Ly6C^{high}$ $Ly6G^-$) typical of monocytes (monocytic MDSCs). Monocytic MDSCs consist of immature myeloid cells with the ability to differentiate into macrophages and dendritic cells. PMN-MDSCs are the largest population of MDSCs in tumor-bearing mice, representing >75% of all MDSCs. They suppress Ag-specific T cell responses, primarily via the release of reactive oxygen species. PMN-MDSCs also have been found in cancer patients. Thus, PMN-MDSCs play a pivotal role in tumor progression. However, the underlying mechanism through which PMN-MDSCs proliferate and infiltrate into tumor sites has been unclear. G-CSF is a cytokine with potent neutrophil-proliferative activity. G-CSF is produced by macrophages, fibroblasts, and endothelial cells. Recently, it was shown that tumor cells are a source of G-CSF (9–12) and that production of G-CSF by tumors is responsible for the recruitment of immunosuppressive PMN-MDSCs, which promote tumor growth via inhibition of antitumor immune responses (13, 14). A vital role for tumor-derived G-CSF in tumor-bearing mice was demonstrated by Waight et al. (13) In addition, depletion of G-CSF resulted in reduced tumor growth in a murine mammary gland cancer 4T1 model. 4T1 cells were previously shown to express a G-CSF transcript; thus, G-CSF is a candidate molecular target for cancer treatment.

ERO1-α is an endoplasmic reticulum (ER)-resident oxidase. ERO1-α and protein disulfide isomerase (PDI) play central roles in disulfide bond formation of secreted and cell surface molecules (15–18). Disulfide bond formation (i.e., oxidative protein folding) is the most common posttranslational modification and is required for proper conformation and function of these molecules. Thus, these secreted and cell surface molecules need to be regulated at the gene expression level, as well as undergo proper posttranscriptional modification. We demonstrated recently that various

*Department of Pathology, Sapporo Medical University, Sapporo 060-8556, Japan; †The United Graduate School of Veterinary Sciences, Yamaguchi University, Yamaguchi 753-8551, Japan; ‡Joint Department of Veterinary Medicine, Tottori University, Tottori 680-8553, Japan; and §Department of Molecular Therapeutics, Center for Food and Medical Innovation, Hokkaido University, Sapporo 001-0021, Japan

ORCID: 0000-0002-0112-8730 (Y.T.).

Received for publication October 3, 2014. Accepted for publication December 3, 2014.

This work was supported in part by a Grant-in-Aid for Scientific Research from The Ministry of Education, Culture, Sports, Science and Technology of Japan.

Address correspondence and reprint requests to Dr. Yasuaki Tamura, Department of Molecular Therapeutics, Center for Food and Medical Innovation, Hokkaido University, Sapporo, Hokkaido 001-0021, Japan. E-mail address: ytamura3566@gmail.com

The online version of this article contains supplemental material.

Abbreviations used in this article: ER, endoplasmic reticulum; KD, ERO1-α knockdown; MDSC, myeloid-derived suppressor cell; OE, ERO1-α overexpressed; PDI, protein disulfide isomerase; PMN, polymorphonuclear; SCR, scrambled shRNA transfected; shRNA, short hairpin RNA; WT, wild-type 4T1.

www.jimmunol.org/cgi/doi/10.4049/jimmunol.1402538

types of tumor cells expressed high levels of ERO1-α and that ERO1-α is a marker of poor prognosis in breast cancer (19). In this article, we demonstrate that ERO1-α plays a pivotal role in PMN-MDSC induction via upregulation of G-CSF production from cancer cells in collaboration with PDI.

Materials and Methods

Cells

The murine breast cancer cell line 4T1 and human breast cancer lines MCF7, BT-474, UACC-893, SK-BR-3, MDA-MB-157, MDA-MB-231, and MDA-MB-468 were purchased from the American Type Culture Collection (Manassas, VA). 4T1, BT-474, and MDA-MB-157 cells were cultured in RPMI 1640 (Sigma-Aldrich, St. Louis, MO); MCF7, MDA-MB-231, and MDA-MB-468 cells were cultured in DMEM (Sigma-Aldrich); UACC-893 cells were cultured in Leibovitz's L-15 (Life Technologies, Carlsbad, CA); and SK-BR-3 cells were cultured in McCoy's 5A media (Life Technologies) supplemented with 10% FCS at 37°C in 5% CO_2. Short hairpin RNA (shRNA) for murine ERO1-α (TR502816) was purchased from OriGene (Rockville, MD) and transfected into 4T1 cells using Lipofectamine RNAiMAX (Life Technologies). Cells were stably propagated under puromycin selection (6 μg/ml). The murine ERO1-α gene fragment was isolated from pCMV6-Entry Vector/mERO1-α (OriGene), digested with BamHI and XhoI, and inserted into an appropriate site of the expression vector pcDNA6/myc-HisA (Invitrogen, Carlsbad, CA). The resulting pcDNA6/mERO1-α or an empty vector as a control was transfected into 4T1 cells using Lipofectamine 2000 (Life Technologies). Cells were stably propagated under blasticidin (5 μg/ml; Life Technologies) selection.

In vivo study

Female BALB/c and BALB/c nu/nu mice (4 wk old) were obtained from The Jackson Laboratory (Bar Harbor, ME) and used at 5 wk of age. Mice were maintained in a specific pathogen–free mouse facility at Sapporo Medical University, according to institutional guidelines for animal use and care. For tumor-formation studies, mice were injected with 3×10^4 4T1 cells, ERO1-α–overexpressed (OE) cells, or ERO1-α–knockdown (KD) cells into the right fourth mammary glands. Tumor growth was measured two or three times/wk in two dimensions, and tumor volume was calculated using the equation $3.14 \times (\text{width}^2 \times \text{length})/6$. Tumor length and width were measured with a caliper.

Treatments

Mice were challenged with 3×10^4 4T1 scrambled shRNA-transfected (SCR) cells. For the depletion of $CD4^+$ and/or $CD8^+$ T cells, mice were injected i.p. with a CD4-specific Ab and/or CD8-specific Ab at 200 μg/mouse on day 3 before and day 1 after tumor challenge. For depletion of $Ly6G^+$ PMN-MDSCs, mice were injected i.p. with Ly6G-specific Ab clone 1A8 (Bio X Cell, West Lebanon, NH) or rat IgG (Sigma-Aldrich) at 100 μg/mouse every 2 d from day 15 after the tumor challenge.

Quantitative RT-PCR analysis and real-time PCR

Total RNA was isolated from cultured cells and normal breast tissues using Isogen reagent (Nippon Gene, Tokyo, Japan) and RNeasy Mini kits (QIAGEN, Valencia, CA) according to manufacturer's instructions. The cDNA mixture was synthesized from 1 μg total RNA by reverse transcription using Superscript III and oligo (dT) primer (Life Technologies) according to the manufacturer's protocol. PCR amplification was performed in 20 μl PCR mixture containing 1 μl cDNA mixture, 0.1 μl Taq DNA polymerase (QIAGEN) and 6 pmol primers. Quantitative RT-PCR was performed with a QuantiTect SYBR Green PCR Kit (QIAGEN) to determine the expression levels of cxcl1, cxcl2, g-csf, and β-actin. Expression values for each sample were normalized to β-actin, and fold levels of the indicated genes represent the mean (± SEM) of replicate reactions. Primer sequences were as follows: β-actin (actb), QuantiTect Mm_Actb_1_SG Primer Assay; cxcl1, QuantiTect Mm_Cxcl1_1_SG Primer Assay; cxcl2, QuantiTect Mm_Cxcl2_1_SG; and g-csf (Csf3), QuantiTect Mm_Csf3_1_SG (QIAGEN). PCR cycles were performed using a StepOne Real-Time PCR System (Life Technologies) with the following cycle conditions: 10 min at 95°C, 45 cycles of 15 s at 95°C and 1 min at 60°C, followed by melting curve analysis. The δ-δ Ct method was used for data analysis.

Real-time relative PCR (real-time PCR) was performed to determine the expression levels of ERO1-α and β-actin. Expression values for each sample were normalized to β-actin, and fold levels of the indicated genes represent the mean (± SEM) of replicate reactions. Primer sequences were as follows: β-actin (ACTB), Hs0160665_g1; and ERO1-α (ERO1L), Hs00205880_m1 (Life Technologies). PCR cycles were performed using a StepOne Real-Time PCR System (Life Technologies) with the following cycle conditions: 2 min at 50°C, 10 min at 95°C, and 40 cycles of 15 s at 95°C and 1 min at 60°C. The ΔΔ Ct method was used for data analysis.

Western blot analysis

Cultured cells were washed in ice-cold PBS, lysed by incubation on ice in a lysis buffer (50 mmol/l Tris-HCl [pH 7.5] 150 mmol/l NaCl, 5 mmol/l EDTA, 1% Nonidet P-40), and cleared by centrifugation at 21,880 × *g* for 30 min at 4°C. For blockade of free thiols, cells were pretreated for 5 min with 10 mM methyl methanethiosulfonate (Pierce, Rockford, IL) in PBS. Postnuclear supernatants were divided and heated for 5 min at 95°C in a nonreducing or reducing SDS sample buffer, resolved by SDS-PAGE, and electrophoretically transferred to polyvinylidene difluoride membranes (Immobilon-P; Millipore, Billerica, MA). The membranes were incubated with blocking buffer (5% nonfat dried milk in PBS) for 30 min at room temperature and then incubated overnight with anti–ERO1-α mAb (Abnova, Taipei, Taiwan), anti-PDI polyclonal Ab (Enzo Life Sciences, Farmingdale, NY), anti–mouse G-CSF (R&D Systems, Minneapolis, MN), or mouse anti–β-actin mAb AC-15 (Sigma-Aldrich). After washing three times with wash buffer (0.1% Tween-20 in TBS), the membranes were reacted with peroxidase-labeled goat anti-rabbit IgG Ab, peroxidase-labeled goat anti-mouse IgG Ab, or peroxidase-labeled rabbit anti-goat Ab (KPL, Gaithersburg, MD) for 3 h. Finally, the signal was visualized using an ECL detection system (Amersham Life Science, Arlington Heights, IL) or an IMMOBILON detection system (Millipore), according to the manufacturers' protocols.

Analyses of leukocytic infiltrates in the tumor and flow cytometry

Mice were injected with 1×10^5 4T1 cells, OE cells, or KD cells into the right fourth mammary glands. Tumor tissues, peripheral blood, spleen, and bone marrow were collected on day 14 after tumor challenge. For analyses of leukocytic infiltrates in the tumor tissue, tumors were mechanically dissociated on a wire mesh by crushing with scissors and digested for 2 to 3 h at 37°C in RPMI 1640 medium supplemented with 5% FBS and Liberase (Roche, Tokyo, Japan; 1 mg/ml). Then, leukocytes were collected by density-gradient centrifugation with Lympholyte-M. Peripheral blood, spleen cells, and bone marrow were hemolyzed by a hemolytic agent. The cells were filtered through 70-μm nylon strainers (BD Biosciences, Bedford, MA), and cell numbers were counted. They were stained with specific markers and analyzed by flow cytometry. All preparations were preincubated with anti-CD16/32 mAb (BD Biosciences, San Diego, CA) to block FcR binding, followed by incubation with a directly conjugated primary Ab. Labeled cells were analyzed using a FACSCalibur flow cytometer (BD, San Jose, CA) and FlowJo software (TreeStar, Ashland, OR). Abs reactive against the following cell surface markers were used (including appropriate isotype controls): PE-labeled CD11b, PerCP/Cy5.5-labeled Ly6G and allophycocyanin-labeled Ly6C (BioLegend, San Diego, CA), and PerCP/Cy5.5-labeled Gr-1 (eBioscience, San Diego, CA).

Immunohistochemistry

Tissue was fixed in neutral 10% buffered formaldehyde, embedded in paraffin, and cut into 5-μm-thick slices for ERO1-α staining. Reactivity of the anti–ERO1-α mAb was determined by perinuclear staining within tumor cells, indicating ER localization. Tissues were frozen with OCT compound (Leica Biosystems, Nussloch, Germany) and cut into 7-μm-thick slices for CD11b and Gr-1 staining. Abs reactive against CD11b and Gr-1 were purchased from BioLegend and eBioscience, respectively. Secondary Abs were purchased from DAKO Japan (Tokyo, Japan). Tissue sections were developed using diaminobenzidine. Images were quantified by counting the number of positively stained cells in five randomly selected fields at ×200 magnification.

ELISA

4T1 cells were plated at 1×10^5 cells/well in six-well plates for 24 or 48 h. All samples were stored at −80°C until assayed. Supernatants were diluted, and mouse CXCL1 (GRO/KC; IBL, Gunma, Japan), mouse CXCL2 (MIP-2α), and mouse G-CSF (R&D Systems) levels were measured using a sandwich ELISA kit. Absorbance was determined at 450 nm.

Statistical analysis

The Student *t* test was used for analysis of two unpaired samples. Statistical differences with regard to depletion of $CD4^+$ and/or CD8 T^+ cells were analyzed by the Dunnett test. Differences in regard to depletion of $Ly6G^+$ PMN-MDSCs were assessed by the Mann–Whitney *U* test. Overall survival rates were calculated by the Kaplan–Meier method, and differences in survival curves were assessed by the log-rank test. All analyses were carried out with StatMate version 3.19 (ATMS, Tokyo, Japan). A p value < 0.05 was regarded as statistically significant. All statistical tests were two sided.

Results

Expression of ERO1-α in breast cancer cell lines and breast cancer tissues

We showed previously that ERO1-α expression was augmented in human breast cancer cell lines and breast cancer tissues (19). In this study, we showed that expression of ERO1-α on breast cancer cell lines was upregulated, regardless of the histological type, compared with the expression in normal breast tissues at the mRNA level (Fig. 1A). Immunohistochemical staining also showed that ERO1-α was preferentially expressed within tumor cells but not normal breast tissue (Fig. 1B, 1C). Our previous study demonstrated that none of the normal breast tissues (71 cases) were positive for ERO1-α staining (19). We observed that ERO1-α showed a patchy staining pattern within cancer nests. Because it was demonstrated that ERO1-α is induced under hypoxic conditions, we assumed that cancer cells residing within hypoxic areas show augmented expression of ERO1-α. Thus, heterogeneity of ERO1-α expression seems to be attributed to the oxygen and blood supply.

Knockdown of ERO1-α by shRNA reduced tumor growth via restoration of antitumor T cell–mediated immunity

To examine the role of ERO1-α in tumor growth, we generated KD cells using shRNA against ERO1-α (Fig. 2A). KD cells did not show differences in a proliferation assay compared with wild-type 4T1 (WT) cells and SCR cells (Supplemental Fig. 1). When BALB/c nu/nu mice were challenged with SCR cells and KD cells, we observed that these two cell lines grew aggressively and at similar rates (Fig. 2B). In contrast, knockdown of ERO1-α retarded tumor growth compared with WT cells in BALB/c mice (Fig. 2C). KD cells also had a survival benefit compared with SCR cells (Fig. 2D). These results suggested that $ERO1\text{-}\alpha^+$ WT or SCR tumor cells inhibited antitumor immunity (i.e., depletion of ERO1-α within tumor cells might restore antitumor immunity). To clarify this, we performed a T cell–depletion assay in vivo. When $CD4^+$ and/or $CD8^+$ T cells were depleted during a tumor-growth assay using KD cells, KD cells showed tumor growth similar to that of SCR cells, indicating that both $CD4^+$ and $CD8^+$ T cells were responsible for the immunogenicity of KD tumor cells (Fig. 3A). Moreover, because some of the mice challenged with KD cells rejected the tumors, we rechallenged these mice with WT cells. All of the mice rechallenged with 4T1 tumor cells rejected tumor cells (Fig. 3B), indicating that KD tumor cells acted as immunogenic tumor cells due to ERO1-α knockdown. Based on these results, both $CD4^+$ and $CD8^+$ T cell–mediated antitumor immunity against 4T1 tumor was dampened by the expression of ERO1-α within 4T1 tumor cells.

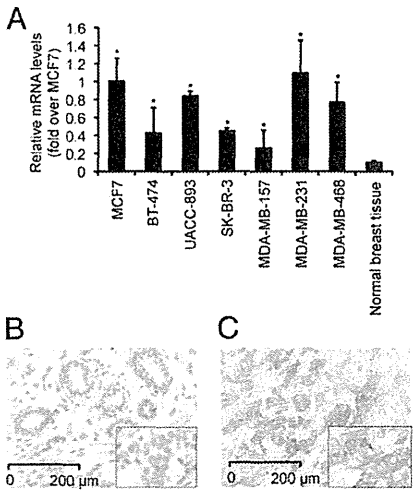

FIGURE 1. Expression of ERO1-α within human breast cancer cell lines was enhanced compared with that in normal breast tissue. **(A)** Human ERO1-α mRNA levels in breast cancer cell lines (luminal type: MCF7, BT-474, UACC-893; HER2 type: SK-BR-3; triple-negative breast cancer: MDA-MB-157, MDA-MB-231, MDA-MB-468) and normal breast tissue, as determined by real-time PCR. Data are mean ± SEM and are representative of three independent experiments. Normal breast tissue (**B**) and breast cancer tissue (**C**) were stained for ERO1-α (original magnification ×100; inset ×200). Representative photomicrographs are shown. $*p <$ 0.05, unpaired Student *t* test.

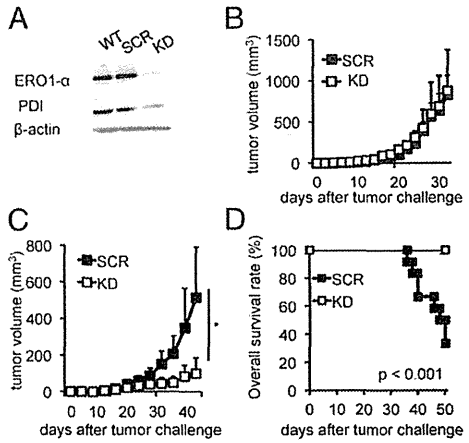

FIGURE 2. Knockdown of ERO1-α within 4T1 cells promoted cellular immunity against 4T1 cells. **(A)** Western blot analysis of WT cells, SCR cells, and KD cells. **(B)** Tumor growth rates of SCR and KD cells in BALB/c nu/nu mice ($n = 5$ mice/group). Data are mean ± SEM. **(C)** Tumor growth rates of SCR and KD cells in BALB/c mice ($n = 11$ mice/group). Data are mean ± SEM. **(D)** Overall survival rates of SCR and KD cells in BALB/c mice ($n = 12$ mice/group, sacrificed when tumor volume was >800 mm^3). Data are mean ± SEM. The experiment was repeated three times with essentially the same results. $*p < 0.01$, unpaired Student *t* test.

Enhanced expression of ERO1-α promotes tumor growth in vivo via suppression of antitumor immunity

To further confirm the effect of ERO1-α on tumor growth and antitumor immunity, we generated an OE 4T1 cell line by introducing murine cDNA of ERO1-α (Fig. 4A). When 4T1 cells transfected with a control vector (mock) and OE cells were inoculated into nude mice, there was no difference in tumor growth rates (Fig. 4B); however, when they were inoculated into BALB/c WT mice, OE tumors grew more aggressively (Fig. 4C, 4D). These results again suggested that expression of ERO1-α suppressed antitumor immunity against the 4T1 tumor.

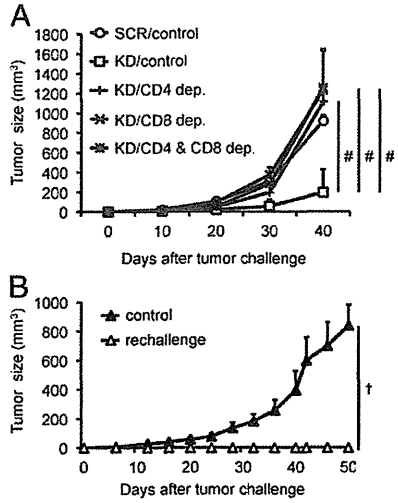

FIGURE 3. Expression of ERO1-α within the tumor suppressed both $CD4^+$ and $CD8^+$ T cell–dependent cellular immunity. **(A)** Mice were challenged with 3×10^4 4T1 SCR cells ($n = 5$ mice) or KD cells ($n = 20$ mice) into the left fourth mammary glands. For the depletion of $CD4^+$ and/or $CD8^+$ T cells, mice were divided into four groups ($n = 5$ mice/group) and injected i.p. with rat IgG (control), a CD4-specific Ab, and/or a CD8-specific Ab (200 μg/mouse) on day 3 before and day 1 after tumor challenge. Data are mean ± SEM. **(B)** Mice that had rejected KD cells were rechallenged with 3×10^4 4T1 cells into the left fourth mammary glands ($n = 5$ mice). As a control, BALB/c mice cells were challenged with 3×10^4 4T1 cells into the left fourth mammary glands ($n = 5$ mice). Tumor length and width were measured with a caliper. Data are mean ± SEM. The experiment was repeated three times with essentially the same results. $^{\#}p < 0.01$, Dunnett test; $^{\dagger}p < 0.001$, Mann–Whitney U test.

PMN-MDSCs accumulate in the spleen, bone marrow, peripheral blood, and tumor of ERO1-α$^+$ 4T1 tumor–bearing mice

Histopathological findings revealed that ERO1-α^+ SCR 4T1 tumor tissues had a large amount of granulocytic infiltrates in the peritumor site, as well as within the tumor mass (Fig. 5A). In clear contrast, KD tumors showed fewer granulocytic infiltrates (Fig. 5B). We compared peritumoral- and intratumoral-infiltrating cells in SCR and KD tumors by immunohistochemical analysis using CD11b mAb and Gr-1 mAb. Although we observed that the major component was $CD11b^+$ $Gr\text{-}1^+$ MDSCs in ERO1-α^+ SCR tumors and KD tumors, the total numbers of both $CD11b^+$ cells and $Gr\text{-}1^+$ cells were increased in SCR tumors (Fig. 5C, 5E, 5G) compared with KD tumors (Fig. 5D, 5F, 5H). Furthermore, we investigated the population of these infiltrates using a flow cytometer. Interestingly, $Ly6G^+$ PMN-MDSCs were more common in the spleen (40.9 versus 17.2%), bone marrow (67.0 versus 57.7%), peripheral blood (57.6 versus 23.7%), and tumor (45.2 versus 27.9%) in SCR tumor–bearing mice compared with KD tumor–bearing mice (Fig. 6, Supplemental Table IA). In contrast, when we compared mice bearing mock tumors and OE tumors, we observed that PMN-MDSC infiltration was higher in OE tumor–bearing mice in the spleen (31.0 versus 18.1%), bone marrow (61.6 versus 60.4%), peripheral blood (50.3 versus 22.3%), and tumor (49.5 versus 37.6%) (Fig. 7, Supplemental Table IB). These results suggested that the expression of ERO1-α within the tumor resulted in the accumulation of PMN-MDSCs throughout the body, including the spleen, bone marrow, peripheral blood, as well as in the tumor, leading to the suppression of antitumor T cell–mediated immunity by PMN-MDSCs.

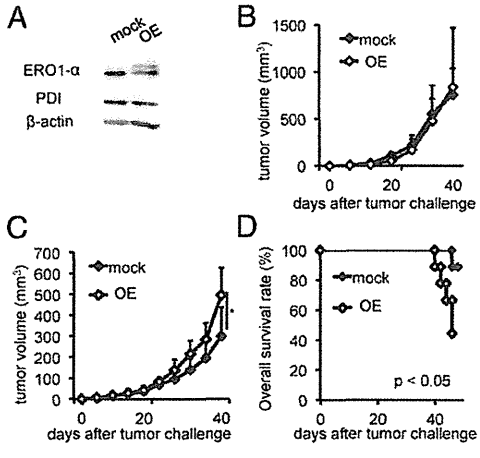

FIGURE 4. Enhanced expression of ERO1-α within 4T1 cells suppressed cellular immunity against 4T1 cells. **(A)** Western blot analysis of mock cells and OE cells. **(B)** Tumor growth rates of mock and OE cells in BALB/c nu/nu mice ($n = 5$ mice/group). Data are mean ± SEM. **(C)** Tumor growth rates of mock and OE cells in BALB/c mice ($n = 8$ mice/group). Data are mean ± SEM. **(D)** Overall survival rates of mock and OE cells in BALB/c mice ($n = 13$ mice/group, sacrificed when tumor volume was >800 mm^3). The experiment was repeated three times with essentially the same results. $^{*}p < 0.05$, unpaired Student t test.

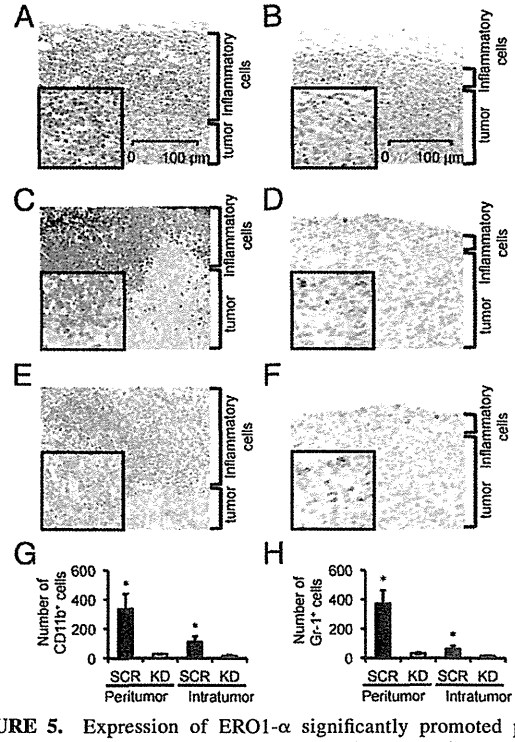

FIGURE 5. Expression of ERO1-α significantly promoted peritumoral and intratumoral infiltration of $CD11b^+$ and $Gr\text{-}1^+$ granulocytic cells. The extent of peritumoral infiltration of inflammatory cells in SCR cells **(A)** was greater than that in KD cells **(B)** (original magnification ×40; inset ×100). Immunohistochemical staining for CD11b (**C** and **D**) and Gr-1 (**E** and **F**) in SCR (C and E) and KD (D and F) tumor tissues (original magnification ×40, inset ×100). $CD11b^+$ cells (**G**) and $Gr\text{-}1^+$ cells (**H**) in peritumoral and intratumoral sites were counted in five fields at ×200 magnification. Data are mean ± SEM. Data are representative of three independent experiments. $^{*}p < 0.001$, Mann–Whitney U test.

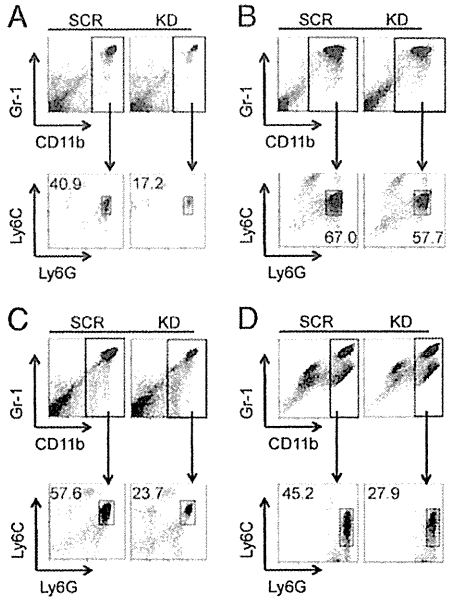

FIGURE 6. Knockdown of ERO1-α within 4T1 cells decreased infiltration of PMN-MDSCs in the body and peritumoral infiltration of PMN-MDSCs. Splenocytes (**A**), bone marrow leukocytes (**B**), peripheral blood leukocytes (**C**), and tumor-infiltrating leukocytes (**D**) that expressed CD11b were divided into $CD11b^+$ $Ly6G^{high}$ and $Ly6C^{int}$ cells by flow cytometric analysis. A total of 3×10^4 events was analyzed for splenocytes and bone marrow and peripheral blood leukocytes, and 2.5×10^4 events were analyzed for tumor-infiltrating leukocytes. Data are representative of three independent experiments.

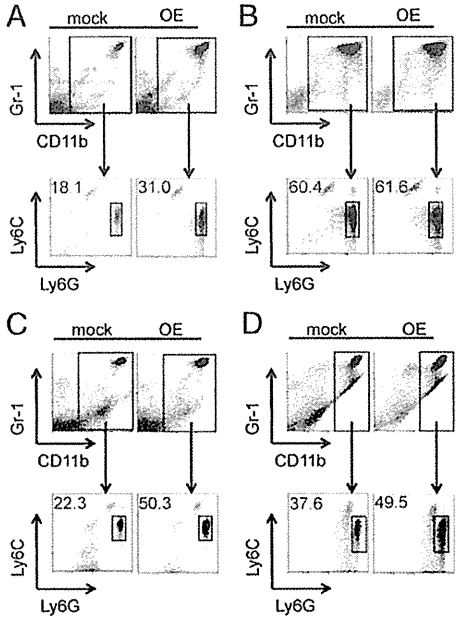

FIGURE 7. Enhanced expression of ERO1-α within 4T1 cells increased the amount of PMN-MDSCs in the body, as well as their peritumoral infiltration. Splenocytes (**A**), bone marrow leukocytes (**B**), peripheral blood leukocytes (**C**), and tumor-infiltrating leukocytes (**D**) that expressed CD11b were classified into $CD11b^+$ $Ly6G^{high}$ and $Ly6C^{int}$ cells by flow cytometric analysis. A total of 2.5×10^4 events was analyzed for each group. Data are representative of three independent experiments.

Depletion of $Ly6G^+$ PMN-MDSCs renders tumor cells immunogenic

To determine whether $Ly6G^+$ MDSCs were the main immunosuppressor cells in the 4T1 tumor system, we depleted $Ly6G^+$ cells during the tumor-growth assay using anti-Ly6G mAb (1A8). Although depletion of $Ly6G^+$ cells seemed incomplete, ~50% of $Ly6G^+$ cells remained in the peripheral blood (Supplemental Fig. 2). Apparently, depletion of $Ly6G^+$ cells retarded SCR tumor growth compared with the growth of isotype-matched control IgG-treated tumors, and SCR tumor growth was almost the same as tumor growth in mice challenged with KD cells (Fig. 8). These results indicated that (tumor-associated) $Ly6G^+$ PMN-MDSCs were the main immunosuppressor cells for ERO1-α^+ 4T1 tumor cells.

Tumor ERO1-α plays a crucial role in the induction and recruitment of PMN-MDSCs

We examined the mechanism of induction of tumor-associated PMN-MDSCs. Because it was demonstrated that G-CSF and GM-CSF induced the proliferation of PMN-MDSCs (1, 13, 14), we measured the production of G-CSF and GM-CSF from 4T1 tumor cells using ELISA. We found that $ERO1^+$ SCR cells produced a large amount of G-CSF compared with the amount produced by KD cells (Fig. 9A). In addition, the production of GM-CSF from SCR cells was greater than that from KD cells, although the difference was not as great as that seen for G-CSF (Supplemental Fig. 3A). Although G-CSF amplifies PMN-MDSCs in the spleen, bone marrow, and peripheral blood, PMN-MDSC recruitment from the circulation to tumor stroma is thought to occur mainly via interaction between the chemokines CXCL1 and CXCL2 (20, 21) and their receptor CXCR2 expressed on PMN-MDSCs (20). Therefore, we compared the concentrations of CXCL1 and CXCL2 in the culture supernatant of each cell line. SCR cells produced a larger amount of CXCL1 and CXCL2 for PMN-MDSC recruitment than did KD cells (Fig. 9B, 9C). In contrast, when we compared mock cells and OE cells, OE cells showed greater production of G-CSF, CXCL1, and CXCL2 (Fig. 9D–F). As expected, PMN-MDSCs in the spleen, bone marrow, and peripheral blood expressed CXCR2 (Supplemental Fig. 3B). These results suggested that tumor-derived G-CSF induced proliferation of PMN-MDSCs, followed by recruitment to the tumor sites by augmented production of CXCL1 and CXCL2, resulted in the inhibition of the antitumor T cell–mediated immune response.

Tumor ERO1-α facilitates the production of G-CSF, CXCL1, and CXCL2 via oxidative folding at the posttranscriptional level

We investigated the role of ERO1-α in the augmented production of G-CSF, CXCL1, and CXCL2. To determine whether the gene expression level was affected by ERO1-α, we compared *g-csf* mRNA expression levels by real-time RT-PCR. The mRNA ex-

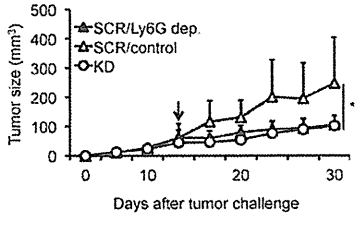

FIGURE 8. Expression of ERO1-α within 4T1 cells promoted tumor growth by increasing the number of PMN-MDSCs in the body. Tumor growth rates in BALB/c mice ($n = 5$ mice/group). Mice were injected i.p. with an Ly6G-specific Ab or rat IgG (100 μg/mouse) every 2 d from day 15 (indicated by ↓) after tumor challenge. Data are mean ± SEM. The experiment was repeated three times with essentially the same results. $^*p < 0.001$, Mann–Whitney U test.

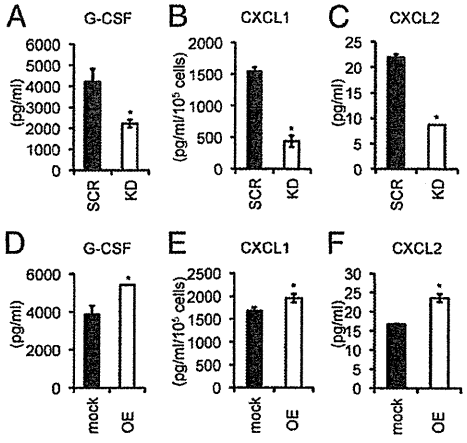

FIGURE 9. Expression of ERO1-α within the tumor was involved in the production of G-CSF, CXCL1, and CXCL2. (**A**) Concentration of G-CSF in the 48-h culture supernatant from SCR or KD cells was measured using ELISA. (**B**) Concentration of CXCL1 in the 24-h culture supernatant from SCR or KD cells was measured using ELISA. (**C**) Concentration of CXCL2 in the 48-h culture supernatant from SCR or KD cells was measured using ELISA. (**D**) Concentration of G-CSF in the 48-h culture supernatant from mock or OE cells was measured using ELISA. (**E**) Concentration of CXCL1 in the 24-h culture supernatant from mock or OE cells was measured using ELISA. (**F**) Concentration of CXCL2 in the 48-h culture supernatant from mock or OE cells was measured using ELISA. Data are mean ± SEM and are representative of three independent experiments. $*p < 0.01$, unpaired Student t test.

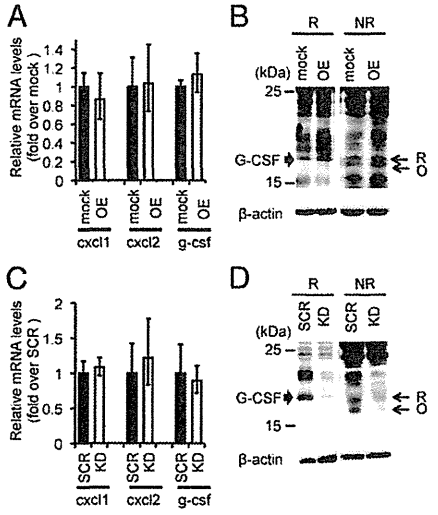

FIGURE 10. Expression of ERO1-α within the tumor facilitated the production of CXCL1, CXCL2, and G-CSF via oxidative folding. Cxcl1, cxcl2, and g-csf mRNA levels in mock and OE cells (**A**) and in SCR and KD cells (**C**) were determined by quantitative RT-PCR. Data are mean ± SEM. Redox status of G-CSF in mock and OE cells (**B**) and in SCR and KD cells (**D**) was examined by Western blotting under reducing (R) or nonreducing (NR) conditions. Reduced form (R) or oxidized form (O) of G-CSF is indicated. Data are representative of three independent experiments.

pression levels were not different in mock cells and OE cells, indicating that the expression of ERO1-α did not influence the *g-csf* gene expression level (Fig. 10A). In addition, we observed that the gene expression levels of *cxcl1* and *cxcl2* were not altered (Fig. 10A). Next, we compared the protein levels using Western blot analysis. Because ERO1-α is known to act as an oxidoreductase, we further investigated the redox states of G-CSF in mock cells and OE cells by Western blot analysis under nonreducing conditions using methyl methanethiosulfonate. We found that the total amount of G-CSF protein in OE cells was greater than that in mock cells under reducing conditions (Fig. 10B). Moreover, we found that ratio of oxidized form (mature form)/ reduced form (immature form) of G-CSF in OE cells was much higher than that in mock cells under nonreducing conditions (Fig. 10B). It was shown that G-CSF has two intramolecular disulfide bonds (22) and that disulfide bond formation is required for G-CSF to exert its biological activity. Taking this into account, these results indicated that tumor ERO1-α plays a pivotal role in the generation of disulfide bonds within G-CSF at the posttranscriptional level but not at the gene expression level. Thus, tumor ERO1-α plays a crucial role in the proper folding of G-CSF, leading to the augmented production of G-CSF. To further confirm our observations, we compared the gene expression levels of *g-csf*, *cxcx1*, and *cxcl2* in SCR and KD cells. As expected, we did not observe any differences in the mRNA levels of these genes between the two cell lines (Fig. 10C). In addition, we compared the redox states of G-CSF in SCR and KD cells and found that the total amount of G-CSF protein was much greater in SCR cells under reducing conditions (Fig. 10D). Furthermore, both the reduced and oxidized forms of ERO1-α were clearly decreased in KD cells compared with SCR cells under nonreducing conditions. We speculated that the decrease in the total amount of G-CSF protein in KD tumor cells occurred via ER-associated degradation, because the immature reduced form of protein is shown to be destined to proteasomal degradation. This will be examined in the future. We concluded that tumor-associated ERO1-α facilitated the oxidative folding of factors including G-CSF, CXCL1, and CXCL2 for the induction and recruitment of PMN-MDSCs, resulting in inhibition of the antitumor T cell response.

Discussion

Oxidative protein folding, characterized by intramolecular disulfide bond formation, is the most common posttranscriptional modification (18). A proper disulfide configuration provides the structural foundation for more nuanced intramolecular folding events that define protein activity (23). Most of the proteins that are secreted or expressed on the cell surface have intramolecular disulfide bonds. Thus, oxidative protein folding is critical for normal cell function and homeostasis. Among the oxidoreductases expressed in the ER, ERO1-α is central to oxidative protein folding, but its expression varies in a tissue-specific manner (19). Moreover, it was shown that ERO1-α is upregulated under hypoxic conditions (24, 25), which are observed frequently in a cancer microenvironment. Furthermore, we showed previously that ERO1-α is overexpressed in various types of cancer cell lines and cancer tissues (19). Because cancer cells may take advantage of factors that are induced within hypoxic environments or at different stages of carcinogenesis, these findings led us to hypothesize that overexpression of ERO1-α is functionally important for tumor cells and prompted further exploration of its role in cancer progression. In this study using a mouse mammary gland cancer 4T1 model, we found that suppression of ERO1-α protein resulted in a dramatic reduction in tumor growth. Because the expression of ERO1-α did not seem to play a major role in tumor cell growth in in vitro or in vivo tumor growth using nude mice, massive infiltration of PMN-MDSCs was considered to contribute to tumor growth in BALB/c mice. In fact, an in vivo depletion assay using anti-Ly6G, anti-CD4, or anti-CD8 mAbs and a tumor rechallenge assay clearly showed that PMN-MDSCs inhibited antitumor T cell responses. Because ERO1-α is a sulfhydryl oxidase (26), it is

unlikely that it would directly induce proliferation of PMN-MDSCs. Therefore, we measured levels of the cytokines and chemokines responsible for the induction or recruitment of PMN-MDSCs in the culture supernatant. 4T1 tumor cells secreted a large amount of G-CSF. In contrast, KD cells showed decreased secretion of G-CSF, CXCL1, and CXCL2. Based on these results, we hypothesized that ERO1-α is involved in the proper oxidative protein folding of G-CSF before it is secreted and that the loss of ERO1-α leads to functionally inactive G-CSF (reduced form), as shown by Western blotting under nonreducing conditions (Fig. 10D). To further confirm that what we observed is a post-transcriptional event, we conducted real-time RT-PCR on SCR cells and KD cells. We did not observe any differences in the mRNA levels of *g-csf, cxcl1,* and *cxcl2* between the two cell lines, suggesting that ERO1-α acted at the posttranslational level. Because ERO1-α–expressing 4T1 cells may affect the function of MDSCs through the production of some cytokines, this possibility should be investigated in the near future.

We reported that ERO1-α is overexpressed in breast cancer tissues and is a useful marker of poor prognosis (19). Many tumors, including breast cancer, have the capacity to promote immune tolerance and escape host immune surveillance (2). Tumors use numerous pathways to inhibit immune responses, including the elaboration of immune inhibitory cytokines, such as IL-10 and TGF-β, as well as inducing host cells to release immune inhibitors. In addition to these mechanisms, immune suppression through MDSCs has a crucial role in promoting tumor progression (1).

In this study using a mouse mammary gland carcinoma 4T1 model, we showed that ERO1-α contributes to suppression of antitumor immunity through upregulation of G-CSF and CXCL1/2 via facilitation of oxidative protein folding. We did not determine whether ERO1-α is solely responsible for the proper oxidative folding of these molecules or whether it cooperates with PDI while these molecules are folding in the ER and Golgi. These questions need to be clarified. Although further research is needed to understand the role of ERO1-α in vivo, the results presented in this article strongly suggest that targeted inhibition of ERO1-α may stall cancer progression.

Disclosures

The authors have no financial conflicts of interest.

References

1. Gabrilovich, D. I., and S. Nagaraj. 2009. Myeloid-derived suppressor cells as regulators of the immune system. *Nat. Rev. Immunol.* 9: 162–174.
2. Nagaraj, S., A. G. Schrum, H. I. Cho, E. Celis, and D. I. Gabrilovich. 2010. Mechanism of T cell tolerance induced by myeloid-derived suppressor cells. *J. Immunol.* 184: 3106–3116.
3. Khaled, Y. S., B. J. Ammori, and E. Elkord. 2014. Increased levels of granulocytic myeloid-derived suppressor cells in peripheral blood and tumour tissue of pancreatic cancer patients. *J. Immunol. Res.* 2014: 879897.
4. Meyer, C., A. Sevko, M. Ramacher, A. V. Bazhin, C. S. Falk, W. Osen, I. Borrello, M. Kato, D. Schadendorf, M. Baniyash, and V. Umansky. 2011. Chronic inflammation promotes myeloid-derived suppressor cell activation blocking antitumor immunity in transgenic mouse melanoma model. *Proc. Natl. Acad. Sci. USA* 108: 17111–17116.
5. Song, C., Y. Yuan, X. M. Wang, D. Li, G. M. Zhang, B. Huang, and Z. H. Feng. 2014. Passive transfer of tumour-derived MDSCs inhibits asthma-related airway inflammation. *Scand. J. Immunol.* 79: 98–104.
6. Kujawski, M., M. Kortylewski, H. Lee, A. Herrmann, H. Kay, and H. Yu. 2008. Stat3 mediates myeloid cell-dependent tumor angiogenesis in mice. *J. Clin. Invest.* 118: 3367–3377.
7. Oh, K., O. Y. Lee, S. Y. Shon, O. Nam, P. M. Ryu, M. W. Seo, and D. S. Lee. 2013. A mutual activation loop between breast cancer cells and myeloid-derived suppressor cells facilitates spontaneous metastasis through IL-6 trans-signaling in a murine model. *Breast Cancer Res.* 15: R79.
8. Markowitz, J., R. Wesolowski, T. Papenfuss, T. R. Brooks, and W. E. Carson, III. 2013. Myeloid-derived suppressor cells in breast cancer. *Breast Cancer Res. Treat.* 140: 13–21.
9. Asano, Y., T. Yokoyama, S. Shibata, S. Kobayashi, K. Shimoda, H. Nakashima, S. Okamura, and Y. Niho. 1997. Effect of the chimeric soluble granulocyte colony-stimulating factor receptor on the proliferation of leukemic blast cells from patients with acute myeloblastic leukemia. *Cancer Res.* 57: 3395–3397.
10. Chakraborty, A., and S. Guha. 2007. Granulocyte colony-stimulating factor/granulocyte colony-stimulating factor receptor biological axis promotes survival and growth of bladder cancer cells. *Urology* 69: 1210–1215.
11. Joshita, S., K. Nakazawa, Y. Sugiyama, A. Kamijo, K. Matsubayashi, H. Miyabayashi, K. Furuta, K. Kitano, and S. Kawa. 2009. Granulocyte-colony stimulating factor-producing pancreatic adenosquamous carcinoma showing aggressive clinical course. *Intern. Med.* 48: 687–691.
12. Savarese, T. M., K. Mitchell, C. McQuain, C. L. Campbell, R. Guardiani, J. Wuu, C. Ollari, F. Reale, B. E. Nelson, A. Chen, and P. J. Quesenberry. 2001. Coexpression of granulocyte colony stimulating factor and its receptor in primary ovarian carcinomas. *Cancer Lett.* 162: 105–115.
13. Waight, J. D., Q. Hu, A. Miller, S. Liu, and S. I. Abrams. 2011. Tumor-derived G-CSF facilitates neoplastic growth through a granulocytic myeloid-derived suppressor cell-dependent mechanism. *PLoS ONE* 6: e27690.
14. Abrams, S. I., and J. D. Waight. 2012. Identification of a G-CSF-Granulocytic MDSC axis that promotes tumor progression. *OncoImmunology* 1: 550–551.
15. Frand, A. R., and C. A. Kaiser. 1999. Ero1p oxidizes protein disulfide isomerase in a pathway for disulfide bond formation in the endoplasmic reticulum. *Mol. Cell* 4: 469–477.
16. Appenzeller-Herzog, C., J. Riemer, B. Christensen, E. S. Sørensen, and L. Ellgaard. 2008. A novel disulphide switch mechanism in Ero1alpha balances ER oxidation in human cells. *EMBO J.* 27: 2977–2987.
17. Appenzeller-Herzog, C., J. Riemer, E. Zito, K. T. Chin, D. Ron, M. Spiess, and L. Ellgaard. 2010. Disulphide production by Ero1α-PDI relay is rapid and effectively regulated. *EMBO J.* 29: 3318–3329.
18. Araki, K., and K. Nagata. 2011. Functional in vitro analysis of the ERO1 protein and protein-disulfide isomerase pathway. *J. Biol. Chem.* 286: 32705–32712.
19. Kutomi, G., Y. Tamura, T. Tanaka, T. Kajiwara, K. Kukita, T. Ohmura, H. Shima, T. Takamaru, F. Satomi, Y. Suzuki, et al. 2013. Human endoplasmic reticulum oxidoreductin 1-α is a novel predictor for poor prognosis of breast cancer. *Cancer Sci.* 104: 1091–1096.
20. Acharyya, S., T. Oskarsson, S. Vanharanta, S. Malladi, J. Kim, P. G. Morris, K. Manova-Todorova, M. Leversha, N. Hogg, V. E. Seshan, et al. 2012. A CXCL1 paracrine network links cancer chemoresistance and metastasis. *Cell* 150: 165–178.
21. Katoh, H., D. Wang, T. Daikoku, H. Sun, S. K. Dey, and R. N. Dubois. 2013. CXCR2-expressing myeloid-derived suppressor cells are essential to promote colitis-associated tumorigenesis. *Cancer Cell* 24: 631–644.
22. Mo, J., A. A. Tymiak, and G. Chen. 2013. Characterization of disulfide linkages in recombinant human granulocyte-colony stimulating factor. *Rapid Commun. Mass Spectrom.* 27: 940–946.
23. Cabibbo, A., M. Pagani, M. Fabbri, M. Rocchi, M. R. Farmery, N. J. Bulleid, and R. Sitia. 2000. ERO1-L, a human protein that favors disulfide bond formation in the endoplasmic reticulum. *J. Biol. Chem.* 275: 4827–4833.
24. Gess, B., K. H. Hofbauer, R. H. Wenger, C. Lohaus, H. E. Meyer, and A. Kurtz. 2003. The cellular oxygen tension regulates expression of the endoplasmic oxidoreductase ERO1-Lalpha. *Eur. J. Biochem.* 270: 2228–2235.
25. May, D., A. Itin, O. Gal, H. Kalinski, E. Feinstein, and E. Keshet. 2005. Ero1-L alpha plays a key role in a HIF-1-mediated pathway to improve disulfide bond formation and VEGF secretion under hypoxia: implication for cancer. *Oncogene* 24: 1011–1020.
26. Araki, K., and K. Inaba. 2012. Structure, mechanism, and evolution of Ero1 family enzymes. *Antioxid. Redox Signal.* 16: 790–799.

Cancer Science
Japanese Cancer Association JCA
Open Access

Heat shock protein 90 targets a chaperoned peptide to the static early endosome for efficient cross-presentation by human dendritic cells

Tsutomu Tanaka,[1,2] Koichi Okuya,[3] Goro Kutomi,[3] Akari Takaya,[1] Toshimitsu Kajiwara,[1] Takayuki Kanaseki,[1] Tomohide Tsukahara,[1] Yoshihiko Hirohashi,[1] Toshihiko Torigoe,[1] Koichi Hirata,[3] Yoshiharu Okamoto,[4] Noriyuki Sato[1] and Yasuaki Tamura[1,5]

[1]Department of Pathology, Sapporo Medical University School of Medicine, Sapporo; [2]United Graduate School of Veterinary Sciences, Yamaguchi University, Yamaguchi; [3]Department of Surgery, Sapporo Medical University School of Medicine, Sapporo; [4]Joint Department of Veterinary Medicine, Tottori University, Tottori; [5]Department of Molecular Therapeutics, Center for Food and Medical Innovation, Hokkaido University, Sapporo, Japan

Key words
Antigen presentation/processing, dendritic cells, heat shock protein, T cells, tumor immunity

Correspondence
Yasuaki Tamura, Department of Molecular Therapeutics, Center for Food and Medical Innovation, Hokkaido University, Kita 21, Nishi 11, Sapporo 001-0021, Japan.
Tel: +81-11-706-9462; Fax: +81-11-706-9463;
E-mail: ytamura3566@gmail.com.

Funding information
Ministry of Health, Labor and Welfare of Japan

Received September 13, 2014; Revised October 23, 2014; Accepted November 4, 2014

Cancer Sci **106** (2015) 18–24

doi: 10.1111/cas.12570

The presentation of an exogenous antigen in a major histocompatibility complex class-I- restricted fashion to CD8$^+$ T cells is called cross-presentation. Heat shock proteins (HSPs) such as Hsp70, gp96, and Hsp90 have been shown to elicit efficient CTL responses by cross-presentation through an as-yet entirely unknown mechanism. Hsp90 is the most abundant cytosolic HSP and is known to act as a molecular chaperone. We have shown that a tumor antigen peptide complexed with Hsp90 could be cross-presented by dendritic cells (DCs) through an endosomal pathway in a murine system. However, it has not been determined whether human DCs also cross-present an Hsp90–peptide complex and induce peptide-specific CTLs. In this study, we found that an Hsp90–cancer antigen peptide complex was efficiently cross-presented by human monocyte-derived DCs and induced peptide-specific CTLs. Furthermore, we observed that the internalized Hsp90–peptide complex was strictly sorted to the Rab5$^+$, EEA1$^+$ static early endosome and the Hsp90-chaperoned peptide was processed and bound to MHC class I molecules through an endosome-recycling pathway. Our data indicate that targeting of the antigen to a "static" early endosome by Hsp90 is essential for efficient cross-presentation.

The generation of specific CD8$^+$ CTLs is thought to play a key role in the control of virus-infected cells and tumors. However, immunization with peptides or recombinant proteins generally fails to elicit CTLs because an immunized antigen (Ag) acts as an exogenous Ag. Generally, an exogenous Ag enters the MHC class II pathway and is presented to CD4$^+$ T cells in the context of MHC class II molecules. However, professional Ag-presenting cells, particularly DCs, can take up exogenous Ag and present them on their MHC class I molecules. This process is called cross-presentation and plays an important role in the control of virus-infected cells and tumor growth.[1] There are two pathways of cross-presentation: cytosolic (endoplasmic reticulum–Golgi-dependent) and vacuolar (endosomal) pathways.[2,3] One of the reasons for inefficiency of a vaccine strategy is that the vaccine Ag is usually administered as an exogenous Ag, and it is therefore difficult to introduce the vaccine Ag into the cross-presentation pathway. To overcome this problem, various methods have been developed to target an exogenous Ag into the endogenous MHC class I-restricted pathway. In our previous studies, we showed that extracellular Hsp90–peptide complexes are efficiently cross-presented through the endosome-recycling pathway.[4] In this Hsp90-mediated cross-presentation, the receptor-dependent endocytosed Hsp90–peptide complex was transferred to the early endosome in which a cysteine protease such as cathepsin S processed the precursor peptide. The resulting MHC class I epitope was transferred onto recycling MHC class I molecules, thereby resulting in the expression of an MHC class I–epitope complex on the cell surface. Furthermore, we have shown that immunization with Hsp90–tumor Ag peptide complexes induces Ag-specific CTL responses and strong antitumor immunity *in vivo*. However, how the Hsp90–peptide complex is sorted out after receptor-dependent endocytosis remains unclear. In the present work, we found that Hsp90 complexed with a human tumor Ag peptide derived from survivin-2B[5,6] is cross-presented by human Mo-DCs resulting in the stimulation of peptide-specific CTLs. In addition, we found that Hsp90 targets a chaperoned Ag peptide into the "static" early endosome within Mo-DCs, resulting in cross-presentation of the antigenic peptide through the recycling pathway.

Materials and Methods

The study protocol was approved by the Clinic Institutional Ethical Review Board of the Medical Institute of Bioregulation,

Sapporo Medical University (Sapporo, Japan). The patients and their families as well as healthy donors gave informed consent for the use of blood samples in our research.

Patient treatment. The patients were vaccinated with survivin-$2B_{80\text{-}88}$ (1 mg) plus Montanide ISA 51 (1 mL; Seppic, Paris, France) s.c. four times at 14-day intervals. In addition, IFN-α (3 000 000 IU; Dainippon-Sumitomo Pharmaceutical Co., Osaka, Japan) was given s.c. twice a week close to the site of vaccination. Hematological examinations were carried out before and after each vaccination.

Induction of human monocyte-derived immature dendritic cells. Autologous monocytes were purified from PBMCs from each patient that were isolated using Lymphoprep (Nycomed, Oslo, Norway). Monocytes (1×10^4/well) in a 24-well plate were cultured in complete RPMI-1640 with 10% FCS and GM-CSF (1000 U/mL) and IL-4 (1000 U/mL) for 7 days. The medium with GM-CSF and IL-4 was gently replaced on day 2 and 4. Human recombinant GM-CSF was a kind gift from Kirin (Tokyo, Japan). Human recombinant IL-4 was purchased from Invitrogen (Carlsbad, CA, USA).

Peptides and proteins. The following peptides were used (underlined sequences representing the precise MHC class I-binding epitope): survivin-$2B_{80\text{-}88}$ (AYACNTSTL); and survivin-$2B_{75\text{-}93}$ (GPGTVAYACNTSTLGGRGG). All peptides were purchased from Sigma-Genosys (Ishikari, Japan). Human Hsp90 was purchased from StressGen (Ann Arbor, MI, USA). Human LDL was purchased from Sigma-Aldrich (St. Louis, MO, USA) and stored at 20 mg/mL in PBS at −80°C.

Antibodies. Confocal laser microscopy was used to detect organelles with specific antibodies: an anti-Rab5 pAb (MBL, Nagoya, Japan) and EEA1 (Abcam, Cambridge, MA, USA) for early endosomes, and anti-LAMP-1 pAb (Santa Cruz Biotechnology, Santa Cruz, CA, USA) for late endosomes/lysosomes. Alexa Fluor 594 (Molecular Probes, Eugene, OR, USA) was used for labeling Hsp90 and LDL.

Generation of Hsp90–peptide complex *in vitro*. As previously described,[4] Hsp90 was mixed with survivin-$2B_{75\text{-}93}$ (GPGTVAYACNTSTLGGRGG) in a 50:1 peptide:protein molar ratio in 0.7 M NaCl containing sodium-phosphate buffer and heated at 45°C for 30 min, then incubated for 30 min at room temperature.

Establishment of survivin-$2B_{80\text{-}88}$-specific CTL clone. We generated survivin-$2B_{80\text{-}88}$-specific CTL clones from a patient with colon cancer (patient 1 in Table 1). After the fourth vaccination, PBMCs were isolated from blood samples by Ficoll–Conray density gradient centrifugation. Phytohemagglutinin blasts were derived from PBMCs by culturing in AIM V medium (Invitrogen) containing 10% human serum, IL-2 (100 U/mL; Takeda Pharmaceutical Co., Osaka, Japan), and PHA (1 mg/mL; Wako Chemicals, Osaka, Japan) for 3 days, followed by washing and cultivation in the presence of IL-2 (100 U/mL) for 4 days. HLA-A*2402-survivin-$2B_{80\text{-}88}$ peptide tetramer-positive (MBL) CTLs were sorted and subsequently cloned to single cells using FACSAria (Becton Dickinson, San Jose, CA, USA). Survivin-$2B_{80\text{-}88}$-specific CTL clones were restimulated with survivin-$2B_{80\text{-}88}$ peptide-pulsed PHA blasts every 7 days in AIM V medium supplemented with 50 U/mL IL-2.

***In vitro* cross-presentation assay.** Human Mo-DCs (1×10^5) were pulsed with Hsp90 (400 μg/mL), survivin-$2B_{75\text{-}93}$ (400 μg/mL) alone, a complex of Hsp90 (100 or 400 μg/mL) and survivin-$2B_{75\text{-}93}$ (100 or 400 μg/mL), a simple mixture of both or survivin-$2B_{80\text{-}88}$ (400 μg/mL) for 2 h at 37°C in 100 μL Opti-MEM and then fixed for 1 min with 0.01% glutaraldehyde. Fixation was stopped by addition of 2 M L-lysine and the cells were washed twice with RPMI-1640 medium and cultured overnight with 1×10^5 survivin-2B peptide-specific CTL clone. Activation of CTLs was measured as IFN-γ production using ELISA. In a dose titration assay, Mo-DCs (1×10^5) were loaded with various doses of survivin-$2B_{80\text{-}88}$ peptide or Hsp90–precursor peptide (survivin-$2B_{75\text{-}93}$) complex for 2 h in 100 μL Opti-MEM and fixed with 0.01% glutaraldehyde. The cells were washed and cultured overnight with 1×10^5 survivin-$2B_{80\text{-}88}$-peptide-specific CTL clone. Interferon-γ in the culture supernatant was measured using ELISA.

***In vitro* stimulation of PBMCs with Mo-DC loaded with Hsp90–precursor peptide complex.** Peripheral blood mononuclear cells were isolated from eight patients suffering from various types of cancer who had been vaccinated with survivin-2B peptide in our clinical study.[7,8] These patients' PBMCs were shown to contain survivin-2B-specific $CD8^+$ T cells. The PBMCs were stimulated with Mo-DCs loaded with survivin-$2B_{80\text{-}88}$ (400 μg/mL), Hsp90 (400 μg/mL), survivin-$2B_{75\text{-}93}$ (400 μg/mL), and Hsp90 (100 or 400 μg/mL)–survivin-$2B_{75\text{-}93}$ (100 or 400 μg/mL) complex in AIM V medium (Life Technologies, Grand Island, NY, USA) containing 10% human serum. Interleukin-2 was added at a final concentration of 50 U/mL on days 2, 4, and 6. On day 7 of culture, the PBMCs were analyzed by tetramer staining and ELISPOT assay.

Assessment of stimulation of Ag-specific CTLs using tetramer assay. The FITC-labeled HLA-A*2402-HIV peptide (RYLRDQQLL) and PE-labeled HLA-A*2402-survivin-$2B_{80\text{-}88}$ peptide tetramers were purchased from MBL. For flow cytometric analysis, PBMCs, which were stimulated *in vitro* as described above, were stained with HIV tetramer or survivin-2B tetramer at 37°C for 20 min. Then a PE-Cy5-conjugated anti-CD8 antibody (eBioscience, San Diego, CA, USA) was added at 4°C for 30 min. Cells were washed twice with PBS. After washing, cells were fixed with 0.5% paraformaldehyde and analyzed by flow cytometry using FACSCalibur and CellQuest software (Becton Dickinson). $CD8^+$ living cells were gated and cells labeled with survivin-2B tetramer were referred to as tetramer-positive cells. The frequency of CTL precursors was calculated as the number of tetramer-positive cells divided by the number of $CD8^+$ T cells.

Assessment of stimulation of Ag-specific CTLs using ELISPOT assay. The ELISPOT plates were coated sterilely overnight with anti-IFN-γ capture antibody (BD Biosciences, San Jose, CA, USA) at 4°C. The plates were then washed once and blocked with AIM V medium containing 10% human serum for 2 h at room temperature. CD8-positive T cells separated from patients' PBMCs (5×10^3 cells/well), which were stimulated *in vitro* as described above, were then added to each well along with HLA-A24-transfected T2 (T2-A24) cells (5×10^4 cells/well) that had been preincubated with survivin-$2B_{80\text{-}88}$ (10 μg/mL) or HIV with an HIV peptide as a negative control. After incubation in a 5% CO_2 humidified chamber at 37°C for 24 h, the wells were washed vigorously five times with PBS and incubated with a biotinylated anti-human IFN-γ antibody (R&D Systems, Minneapolis, MN, USA) and HRP-conjugated avidin. Spots were visualized and analyzed using KS ELISPOT (Carl Zeiss, Jena, Germany).

Immunocytological localization of Hsp90–survivin-$2B_{75\text{-}93}$ peptide complex. Heat shock protein 90 and LDL were conjugated with Alexa Fluor 594 (Molecular Probes) according to the manufacturer's instructions. Monocyte-derived DCs were incubated at 37°C with Alexa Fluor 594-labeled Hsp90 (20 μg) complexed with survivin-$2B_{75\text{-}93}$ peptide (20 μg) for 1 h.

Table 1. Quantitation of survivin-2B-specific CD8$^+$ T cells by tetramer assay

Patient no.	Tumor	Survivin-$2B_{80-88}$-specific CD8$^+$ T cell frequency (tetramer staining)						
		In vitro stimulation	(–)	Survivin-$2B_{80-88}$	Hsp90	Survivin-$2B_{75-93}$	Hsp90–survivin-$2B_{75-93}$	Effect
1	Colon		0.06	4.87	4.47	3.24	8.47	††
2	Colon		0.32	2.87	0.77	4.01	1.30	No
3	Pancreas		0.70	6.27	1.70	1.88	6.64	††
4	Pancreas		0.48	4.56	0.84	1.28	3.02	†
5	Ampulla of Vater		1.27	4.60	0.97	2.24	6.50	††
6	Breast		3.59	3.78	3.00	3.06	3.82	††
7	Breast		3.98	3.91	1.94	2.28	6.19	††
8	Breast		2.76	3.92	2.91	2.08	6.07	††

†Frequency of survivin-2B-specific CD8$^+$ T cells stimulated with heat shock protein 90 (Hsp90)–survivin-$2B_{75-93}$ peptide complex was increased compared with stimulation with survivin-$2B_{75-93}$ precursor peptide. ††Frequency of survivin-2B-specific CD8$^+$ T cells stimulated with Hsp90–survivin-$2B_{75-93}$ peptide was increased compared with stimulation with both survivin-$2B_{80-88}$ peptide and survivin-$2B_{75-93}$ peptide. (–), negative control; No, no effect.

Following incubation, cells were washed twice with ice-cold PBS and fixed with ice-cold acetone for 1 min. Organelles were stained with an anti-Rab5 pAb and EEA1 mAb for early endosomes and anti-LAMP-1 pAb for late endosomes followed by Alexa 488-conjugated goat anti-rabbit IgG (Molecular Probes) or anti-mouse IgG (Molecular Probes) and then visualized with a Bio-Rad MRC1024ES confocal scanning laser microscope system (Bio-Rad, Richmond, CA, USA). For evaluation of colocalization, a single z-plane of one cell was evaluated. For each protein and organelle combination, a total of 150 cells (50 cells from three independent experiments) were analyzed.

Inhibition studies. Monocyte-derived DCs were pre-incubated with chloroquine (Sigma-Aldrich) or primaquine (ICN Biomedicals, Irvine, CA, USA) at 37°C for 2 h, and then loaded with survivin-$2B_{80-88}$ peptide alone or Hsp90–precursor peptide (survivin-$2B_{75-93}$) complex for 2 h. The Mo-DCs were then fixed, washed, and cultured overnight with survivin-$2B_{80-88}$-specific CTL clone. Activation of CTLs was measured as IFN-γ production using ELISA.

Statistical analysis. All experiments were independently carried out three times in triplicate. Results are shown as means + SEM. Comparisons between two groups were performed using Student's *t*-test, with a *P*-value < 0.05 considered to be statistically significant.

Results

Heat shock protein 90–survivin-$2B_{75-93}$ peptide complex is cross-presented by Mo-DCs *in vitro*. We first examined whether human Hsp90 facilitated cross-presentation of the chaperoned precursor peptide by human Mo-DCs. The Mo-DCs were pulsed with Hsp90 alone, the survivin-$2B_{75-93}$ precursor peptide alone, a simple mixture of both, a complex of them generated *in vitro* at double concentration, or survivin-$2B_{80-88}$ peptide (for positive control) for 2 h at 37°C and then fixed, washed, and cultured with survivin-$2B_{80-88}$-specific CTL clone. The Hsp90–survivin-$2B_{75-93}$ precursor peptide complex elicited a significant amount of IFN-γ production both at 100 and 100 μg/mL, whereas Hsp90 alone, survivin-$2B_{75-93}$ precursor peptide alone, or a simple mixture of both did not induce IFN-γ production by CTLs (Fig. 1a). Strikingly, IFN-γ production induced by Hsp90–survivin-2B precursor peptide complex was much greater than that induced by survivin-2B peptide. These results indicated that cross-presentation of survivin-2B-derived peptide was enhanced when an exogenous precursor peptide was complexed to Hsp90. To confirm these observations, we compared the efficacy of CTL activation between survivin-

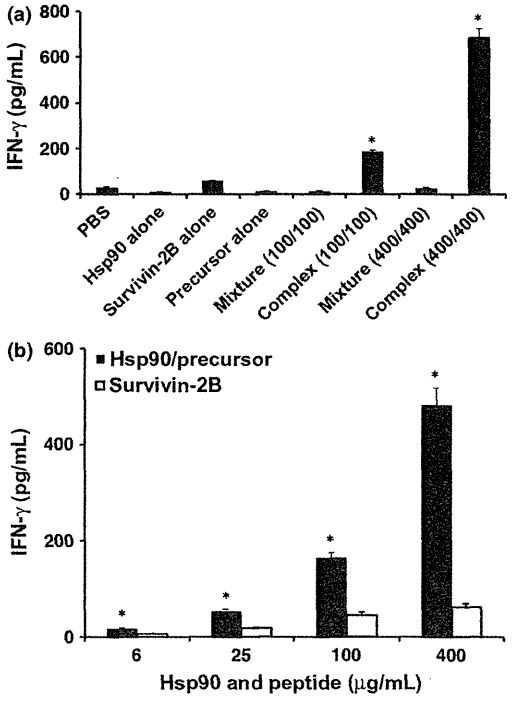

Fig. 1. Cross-presentation of heat shock protein 90 (Hsp90)-chaperoned peptides by human monocyte-derived dendritic cells (Mo-DCs). (a) Human Mo-DCs (1×10^5) were pulsed with Hsp90 (400 μg/mL), precursor peptide survivin-$2B_{75-93}$ (400 μg/mL) alone, a complex of Hsp90 (100 or 400 μg/mL) and survivin-$2B_{75-93}$ (100 or 400 μg/mL), a simple mixture of both, or survivin-$2B_{80-88}$ peptide (for positive control) for 2 h at 37°C and then fixed with 0.01% glutaraldehyde, washed, and cultured with survivin-$2B_{80-88}$-specific CTL clone (1×10^5/well). Activation of CTLs was measured as γ-interferon (IFN-γ) production using ELISA. (b) Mo-DCs (1×10^5) were loaded with various doses of survivin-$2B_{80-88}$ peptide (6, 25, 100, and 400 μg/mL) or Hsp90–survivin-$2B_{75-93}$ precursor peptide complex (6/6, 25/25, 100/100, and 400/400 μg/mL) for 2 h in 100 μL Opti-MEM and fixed with 0.01% glutaraldehyde. The cells were washed and cultured overnight with 1×10^5 survivin-$2B_{80-88}$-specific CTL clone. Activation of CTLs was measured as IFN-γ production using ELISA. Data are shown as means + SEM of three independent experiments. *$P < 0.01$.

$2B_{80-88}$ peptide and Hsp90–survivin-$2B_{75-93}$ precursor peptide complex in a dose titration assay (Fig. 1b). We observed that stimulation of the survivin-$2B_{80-88}$-specific CTL clone with Hsp90–survivin-$2B_{75-93}$ precursor peptide complex was more effective than stimulation with survivin-$2B_{80-88}$ peptide at any dose.

Peptide-specific precursor CTLs are activated by cross-presentation of Hsp90–peptide complex. As we had shown that the Hsp90–survivin-$2B_{75-93}$ precursor peptide complex was efficiently cross-presented, we next examined whether cross-presentation of Hsp90–peptide complex could activate and expand peptide-specific memory $CD8^+$ T cells from patients who had been vaccinated with survivin-2B peptide with incomplete Freund's adjuvant. Activated and expanded survivin-2B-specific $CD8^+$ T cells were detected by tetramer staining. As shown in Figure 2, the survivin-$2B_{75-93}$ precursor peptide chaperoned by Hsp90 was able to activate and expand survivin-2B-specific memory $CD8^+$ T cells more vigorously than was the precursor peptide alone. Interestingly, peptide-specific T-cell frequency was higher when stimulated with Hsp90–survivin-$2B_{75-93}$ precursor peptide complex than that with survivin-$2B_{80-88}$ peptide, indicating that a long peptide chaperoned by Hsp90 was efficiently cross-presented and was able to stimulate peptide-specific $CD8^+$ T cells. To confirm these observations, we compared the efficacy of activation of survivin-2B-specific memory $CD8^+$ T cells by stimulation with survivin-$2B_{80-88}$, survivin-$2B_{75-93}$ precursor peptide, or Hsp90–survivin-$2B_{75-93}$ precursor peptide complex in eight patients. As shown in Table 1, stimulation with Hsp90–survivin-$2B_{75-93}$ complex could expand survivin-2B-specific memory $CD8^+$ T cells from seven out of eight patients compared with stimulation with survivin-$2B_{75-93}$. More importantly, in six out of eight patients, stimulation with Hsp90–survivin-$2B_{75-93}$ complex expanded survivin-2B-specific memory $CD8^+$ T cells more efficiently compared with stimulation with survivin-$2B_{80-88}$.

Memory $CD8^+$ T cells activated by cross-presentation of Hsp90–peptide complex become functional peptide-specific CTLs. To further confirm whether survivin-2B-specific $CD8^+$ T cells activated by Hsp90-mediated cross-presentation were functional or not, we carried out an ELSPOT assay using $CD8^+$ T cells from a patient who had been vaccinated with survivin-2B peptide with incomplete Freund's adjuvant. Figure 3 shows that stimulation of $CD8^+$ T cells from the patient with Hsp90–survivin-$2B_{75-93}$ precursor peptide complex clearly increased functionally positive survivin-2B-specific $CD8^+$ T cells compared with stimulation with survivin-$2B_{75-93}$ precursor peptide or survivin-$2B_{80-88}$ peptide. When $CD8^+$ T cells from the patient were stimulated with Hsp90 (400 μg/mL)–precursor peptide (400 μg/mL) complex, the number of IFN-γ-positive spots was less than that of $CD8^+$ T cells stimulated with Hsp90 (100 μg/mL)–precursor peptide (100 μg/mL) complex. These results were due to the formation of fused large spots that were observed when stimulated with Hsp90 (400 μg/mL)–precursor peptide (400 μg/mL) complex and therefore the number of ELISPOT counted became smaller than that of Hsp90 (100 μg/mL)–precursor peptide (100 μg/mL) complex. These findings indicated that Hsp90–peptide complex is efficiently cross-presented by human Mo-DCs and is capable of stimulating peptide-specific CTLs.

Immunocytological localization of Hsp90–survivin$2B_{75-93}$ peptide complex. For further support of the above-described results, we investigated the intracellular routing of Hsp90 after uptake of it in DCs, using confocal laser microscopy. The Mo-DCs were incubated with Alexa 594-labeled Hsp90–survivin$2B_{75-93}$ peptide complex for 1 h. Following incubation, the cells were fixed and stained with antibodies against markers for organelle structures including EEA1, Rab5, and LAMP-1. Alexa 594-labeled Hsp90–peptide complex was detected in $EEA1^+$ and $Rab5^+$-early endosomes but not in lysosomes (Fig. 4a). Quantitative analysis of the colocalization between the exogenous Hsp90–peptide complex and Rab5, EEA1, and LAMP1 revealed average colocalization incidences of 78.0%, 88.7%, and 7.3%, respectively, providing further evidence that the exogenous Hsp90–peptide complex was delivered to the endosome-recycling pathway (Fig. 4b). We also examined the dynamics of Alexa 594-labeled LDL as a positive control protein for the dynamic early endosomal pathway (Fig. 5). Alexa594-labeled soluble LDL localized to the $Rab5^+$-early endosome as well as the LAMP-1^+-late endosome/lysosome,

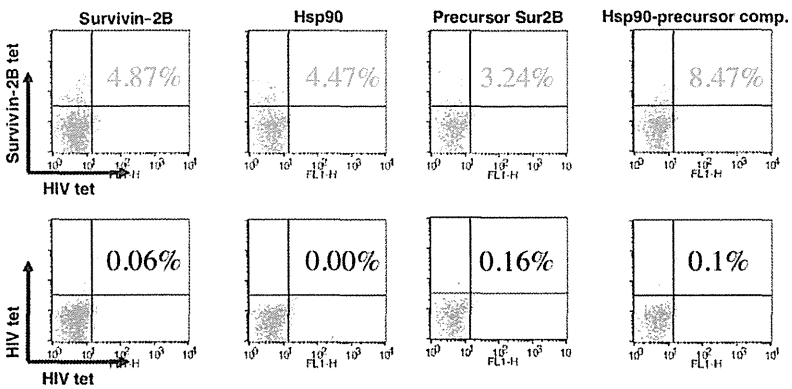

Fig. 2. Peptide-specific precursor CTLs were activated by cross-presentation of heat shock protein 90 (Hsp90)–peptide complex. PBMCs were isolated from patient 1 suffering from colon cancer (Table 1) who had been vaccinated with survivin-$2B_{80-88}$ peptide in our clinical study. The patient's PBMCs were shown to contain the survivin-2B-specific $CD8^+$ T cells. PBMCs were stimulated with human monocyte-derived dendritic cells loaded with survivin-$2B_{80-88}$ (400 μg/mL), Hsp90 (400 μg/mL), survivin-$2B_{75-93}$ precursor peptide (400 μg/mL), and Hsp90 (400 μg/mL)–survivin-$2B_{75-93}$ precursor peptide (400 μg/mL) complex in AIM V medium containing 10% human serum and interleukin-2 (50 U/mL) for 7 days. The stimulated PBMCs were stained with HIV tetramer (tet) or survivin-2B tetramer at 37°C for 20 min. Then a phycoerythrin-Cy5-conjugated anti-CD8 antibody was added at 4°C for 30 min. Cells were washed twice with PBS. After washing, cells were fixed with 0.5% paraformaldehyde and analyzed by flow cytometry using FACSCalibur and CellQuest software. $CD8^+$ living cells were gated, and cells labeled with survivin-2B tetramer were referred to as tetramer-positive cells. The frequency of CTL precursors was calculated as the number of tetramer-positive cells divided by the number of $CD8^+$ cells. Data are shown as means + SEM of three independent experiments. $^*P < 0.01$.

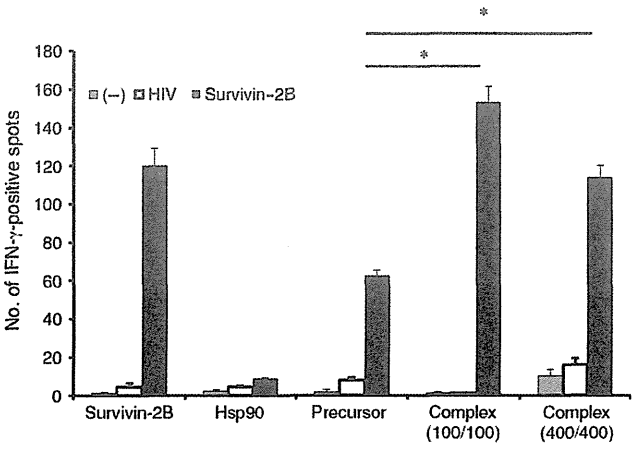

Fig. 3. Memory CD8$^+$ T cells activated by cross-presentation of heat shock protein 90 (Hsp90)–peptide complex became functional peptide-specific CTLs. CD8$^+$ T cells separated from PBMCs (5×10^3 cells/well) from patient 1 (Table 1) were stimulated with human monocyte-derived dendritic cells loaded with survivin-2B$_{80\text{-}88}$ (400 μg/mL), Hsp90 (400 μg/mL), precursor peptide survivin-2B$_{75\text{-}93}$ (400 μg/mL), and Hsp90 (100 or 400 μg/mL)–survivin-2B$_{75\text{-}93}$ (100 or 400 μg/mL) complex, were added to each well along with HLA-A24-transfected T2 (T2-A24) cells (5×10^4 cells/well) that had been preincubated with survivin-2B$_{80\text{-}88}$ (10 μg/mL) or HIV with an HIV peptide as a negative control (–). After incubation in a 5% CO_2 humidified chamber at 37°C for 24 h, the wells were washed vigorously five times with PBS and incubated with a biotinylated anti-human γ-interferon (IFN-γ) antibody and HRP-conjugated avidin. Spots were visualized and analyzed using KS ELISPOT. Data are shown as means + SEM of three independent experiments. *$P < 0.01$.

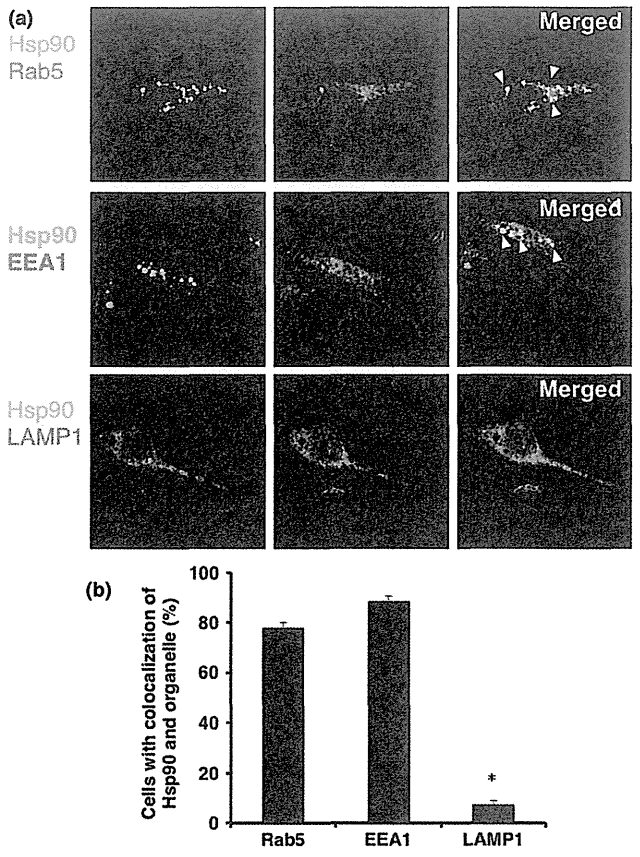

Fig. 4. Heat shock protein 90 (Hsp90)–survivin-2B$_{75\text{-}93}$ precursor peptide complex localized to static early endosomes within human monocyte-derived dendritic cells (Mo-DCs). (a) Human Mo-DCs were incubated at 37°C with Alexa 594-labeled Hsp90–survivin-2B$_{75\text{-}93}$ peptide complex for 1 h and then washed and fixed. Organelles were stained with an anti-EEA1 mAb for early endosomes, anti-Rab5 polyclonal antibody for early endosomes, and anti-LAMP-1 polyclonal antibody for late endosomes/lysosomes followed by Alexa 488-conjugated goat anti-rabbit IgG or anti-mouse IgG and were visualized with confocal laser microscopy. Arrowheads indicate colocalization of the internalized Hsp90–survivin-2B$_{75\text{-}93}$ peptide complex and each organelle. (b) To quantify the percentage of colocalization, a single z-plane of one cell was evaluated. For each protein and organelle combination, a total of 150 cells (50 cells from three independent experiments) were analyzed. Data are shown as means + SEM of three independent experiments. *$P < 0.01$.

but not to the EEA1$^+$-compartment, thus indicating the dynamic endosomal pathway. These results indicated that the Hsp90–peptide complex was sorted into the static endosomal pathway, not the dynamic endosomal pathway, within human Mo-DCs. In contrast, the soluble LDL protein, which underwent degradation, was translocated to the dynamic endosomal pathway. These results suggested that targeting to the "static" early endosome was required for efficient cross-presentation by Mo-DCs.

Heat shock protein 90–peptide complex is cross-presented by human DCs through an endosome-recycling pathway. We then examined whether Hsp90–precursor peptide complex was cross-presented by human Mo-DCs through an endosomal pathway after targeting to the static early endosome. We used chloroquine for inhibition of endosomal acidification and primaquine for inhibition of the membrane recycling pathway. As shown in Figure 6(a), Mo-DCs that were pre-incubated with increasing concentrations of chloroquine completely blocked cross-presentation of Hsp90–survivin-2B$_{75\text{-}93}$ precursor peptide complex but had no substantial effect on survivin-2B$_{80\text{-}88}$ peptide presentation. These results indicated that cross-presentation of Hsp90–precursor peptide complex depended on endosomal acidification, possibly including proteolysis by endosomal proteases. Moreover, Mo-DC incubated with primaquine could not present the Hsp90-chaperoned precursor peptide-derived survivin-2B$_{80\text{-}88}$ peptide to CTL (Fig. 6b). These results indicated that the Hsp90-chaperoned precursor peptide or processed peptide entered recycling endosomes and were transferred onto recycling MHC class I molecules.

Discussion

It has been shown that immunization with tumor-derived HSPs or HSPs complexed with an Ag peptide/protein elicits tumor- or Ag-specific CD8$^+$ T cell responses.[1,9] Importantly, it has been shown that Hsp70–Ag and gp96–Ag complexes facilitate Ag presentation in association with MHC class I molecules.[10–13] Recently, we[3,4] and Calderwood's group[14] have shown that Hsp90 also acted as an excellent navigator for associated antigens to enter the cross-presentation pathway in the murine system. We here showed that human Hsp90–cancer Ag peptide complex was efficiently cross-presented by human Mo-DCs. These results hold promise for the development of a safe and efficient immunomodulator for cancer immunotherapy. More importantly, we showed that translocation of the Hsp90–Ag complex into the static early endosome after endocytosis was crucial for efficient cross-presentation. It has been shown that the pathway for cross-presentation is comprised of two distinct intracellular routes, a proteasome–TAP-dependent pathway and an endosome-recycling pathway.[2,3] Recent studies have revealed the pathway in which peptide exchange onto recy-

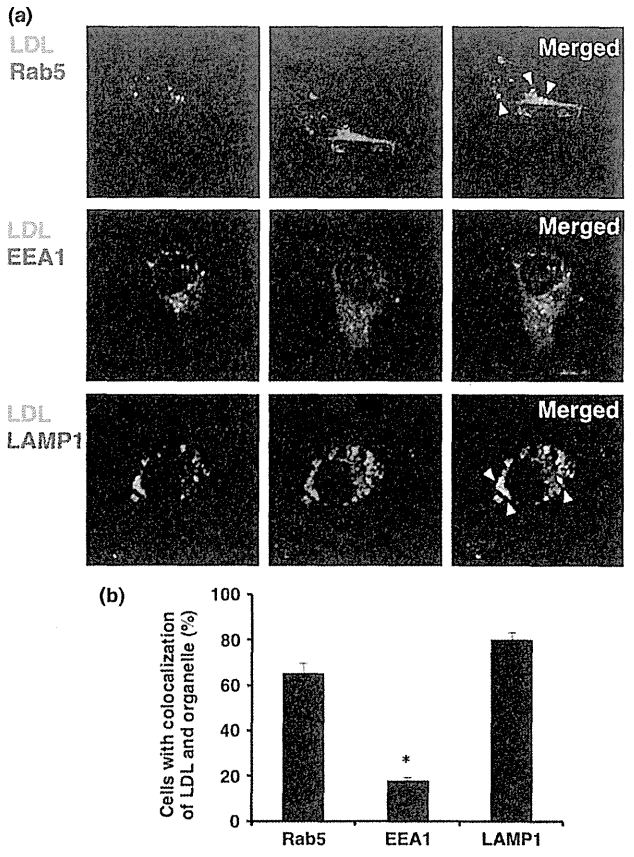

Fig. 5. Low-density lipoprotein (LDL) was targeted to the dynamic early endosome followed by translocation to the late endosome/lysosome for degradation. (a) Human monocyte-derived dendritic cells were incubated at 37°C with Alexa 594-labeled LDL. Organelles were stained with an anti-EEA1 mAb, anti-Rab5 polyclonal antibody, and anti-LAMP-1 polyclonal antibody, followed by Alexa 488-conjugated goat anti-rabbit IgG or anti-mouse IgG. Arrowheads indicate colocalization of internalized LDL and each organelle. (b) To quantify the percentage of colocalization, a single z-plane of one cell was evaluated. For each protein and organelle combination, a total of 150 cells (50 cells from three independent experiments) were analyzed. Data are shown as means + SEM of three independent experiments. $^*P < 0.01$.

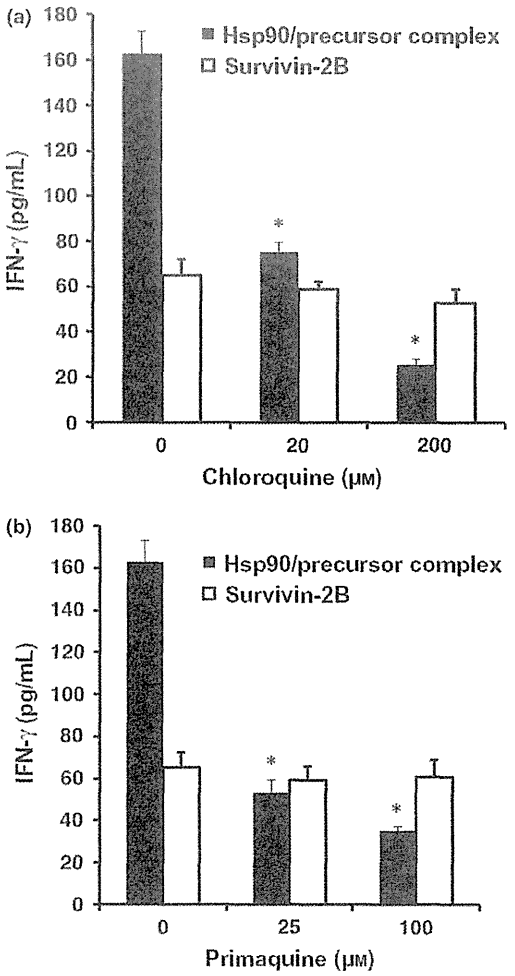

Fig. 6. Heat shock protein 90 (Hsp90)–peptide complex is cross-presented through an endosome-recycling pathway. Human monocyte-derived dendritic cells (Mo-DCs) were pre-incubated with chloroquine (a) or primaquine (b) at 37°C for 2 h and then loaded with survivin-$2B_{80\text{-}88}$ peptide alone or Hsp90–survivin-$2B_{75\text{-}93}$ precursor peptide complex for 2 h. The Mo-DCs were then fixed, washed, and cultured overnight with survivin-$2B_{80\text{-}88}$-specific CTL clone. Activation of CTL was measured as γ-interferon (IFN-γ) production using ELISA.

cling MHC class I molecules occurs within early endosomal compartments.[15] We have shown that Hsp90–peptide complex-mediated[4] and ORP150–peptide complex-mediated[16] cross-presentation was independent of TAP and was sensitive to primaquine, indicating that sorting of peptides onto MHC class I occurs through an endosome-recycling pathway. Lakadamyali *et al.*[17] have shown that early endosomes are comprised of two distinct populations: a dynamic population that is highly mobile on microtubules and matures rapidly toward the late endosome, and a static population that matures much more slowly. Cargos destined for degradation, including LDL, epidermal growth factor, and influenza virus, are internalized and targeted to the $Rab5^+$, $EEA1^-$-dynamic population of early endosomes as we have observed using LDL, thereafter trafficking to $Rab7^+$-late endosomes. In contrast, the recycling ligand transferrin is delivered to $Rab5^+$, $EEA1^+$-static early endosomes, followed by translocation to $Rab11^+$-recycling endosomes. Furthermore, Burgdorf *et al.*[18] clearly indicated that a mannose receptor introduced OVA specifically into an $EEA\text{-}1^+$, $Rab5^+$-stable early endosomal compartment for subsequent cross-presentation. In contrast, pinocytosis conveyed OVA to lysosomes for class II presentation. Of interest, OVA endocytosed by a scavenger receptor did not colocalize with EEA1 but colocalized with LAMP-1 in lysosomes, leading to presentation in the context of MHC class II molecules. We showed that the human Hsp90–peptide complex is targeted into $Rab5^+$, $EEA1^+$-early endosomes after internalization by Mo-DCs, suggesting that preferential sorting to the "static" endosome is necessary for cross-presentation of Hsp90–peptide complexes. In contrast, soluble LDL protein was targeted to the $EEA1^-$ and $LAMP\text{-}1^+$-dynamic early endosome–late endosome/lysosome pathway, leading to degradation and presentation in the context of MHC class II molecules. These findings suggested that Hsp90 shuttled the chaperoned precursor peptide into the static endosome-recycling pathway, preventing further degradation, followed by transfer of the peptide onto recycling MHC class I molecules. Together, our findings indicate that the role